



# A Damaged-Informed Lung Ventilator Model for Ventilator Waveforms

Deepak K. Agrawal<sup>1,2\*</sup>, Bradford J. Smith<sup>1,3</sup>, Peter D. Sottile<sup>4</sup> and David J. Albers<sup>1,2,5\*</sup>

<sup>1</sup> Department of Bioengineering, University of Colorado Denver|Anschutz Medical Campus, Aurora, CO, United States,

<sup>2</sup> Section of Informatics and Data Science, Department of Pediatrics, School of Medicine, University of Colorado Anschutz Medical Campus, Aurora, CO, United States, <sup>3</sup> Section of Pulmonary and Sleep Medicine, Department of Pediatrics,

University of Colorado Anschutz Medical Campus, Aurora, CO, United States, <sup>4</sup> Division of Pulmonary Sciences and Critical Care Medicine, Department of Medicine, University of Colorado School of Medicine, Aurora, CO, United States,

<sup>5</sup> Department of Biomedical Informatics, Columbia University, New York, NY, United States

## OPEN ACCESS

### Edited by:

Walter Araujo Zin,  
Federal University of Rio de Janeiro,  
Brazil

### Reviewed by:

Norihiro Shinozuka,  
Chibaken Saiseikai Narashino  
Hospital, Japan  
Carmen Silvia Valente Barbas,  
University of São Paulo, Brazil

### \*Correspondence:

Deepak K. Agrawal  
agwal.deepak@gmail.com  
David J. Albers  
David.Albers@cuanschutz.edu

### Specialty section:

This article was submitted to  
Respiratory Physiology,  
a section of the journal  
*Frontiers in Physiology*

Received: 11 June 2021

Accepted: 01 September 2021

Published: 01 October 2021

### Citation:

Agrawal DK, Smith BJ, Sottile PD  
and Albers DJ (2021) A  
Damaged-Informed Lung Ventilator  
Model for Ventilator Waveforms.  
*Front. Physiol.* 12:724046.  
doi: 10.3389/fphys.2021.724046

Motivated by a desire to understand pulmonary physiology, scientists have developed physiological lung models of varying complexity. However, pathophysiology and interactions between human lungs and ventilators, e.g., ventilator-induced lung injury (VILI), present challenges for modeling efforts. This is because the real-world pressure and volume signals may be too complex for simple models to capture, and while complex models tend not to be estimable with clinical data, limiting clinical utility. To address this gap, in this manuscript we developed a new damaged-informed lung ventilator (DILV) model. This approach relies on mathematizing ventilator pressure and volume waveforms, including lung physiology, mechanical ventilation, and their interaction. The model begins with nominal waveforms and adds limited, clinically relevant, hypothesis-driven features to the waveform corresponding to pulmonary pathophysiology, patient-ventilator interaction, and ventilator settings. The DILV model parameters uniquely and reliably recapitulate these features while having enough flexibility to reproduce commonly observed variability in clinical (human) and laboratory (mouse) waveform data. We evaluate the proof-in-principle capabilities of our modeling approach by estimating 399 breaths collected for differently damaged lungs for tightly controlled measurements in mice and uncontrolled human intensive care unit data in the absence and presence of ventilator dyssynchrony. The cumulative value of mean squares error for the DILV model is, on average,  $\approx$ 12 times less than the single compartment lung model for all the waveforms considered. Moreover, changes in the estimated parameters correctly correlate with known measures of lung physiology, including lung compliance as a baseline evaluation. Our long-term goal is to use the DILV model for clinical monitoring and research studies by providing high fidelity estimates of lung state and sources of VILI with an end goal of improving management of VILI and acute respiratory distress syndrome.

**Keywords:** ventilator-induced lung injury, ventilator waveform, mathematical model, acute respiratory distress syndrome, statistical inference

## INTRODUCTION

Mechanical ventilation is a life-saving therapy for patients who are unable to perform gas exchange by breathing on their own. When used incorrectly, mechanical ventilation has the potential to worsen lung injury through barotrauma, volutrauma, and atelectrauma that are collectively referred to as ventilator-induced lung injury (VILI). Furthermore, while the patient and ventilator always interact, when the patient and ventilator are dyssynchronous—known as ventilator dyssynchrony (VD)—the timing and delivery of a mechanical breath in response to a patient effort may lead VILI and poor outcomes (Sottile et al., 2018a). There are conditions or syndrome such as acute respiratory distress syndrome (ARDS) that carry a high mortality rate and may be exacerbated, or even caused, by VILI (Ware and Matthay, 2000; Phua et al., 2009; Force et al., 2012; Amato et al., 2015). Therefore, identifying lung-protective ventilation to reduce VILI is both important and challenging because the oxygenation needs are often in opposition to safe ventilation, leading to a complex interplay between the underlying pulmonary pathophysiology, ventilator mechanics, and patient-ventilator interactions (Chiumello et al., 2008; Gilstrap and MacIntyre, 2013; Blanch et al., 2015; Yoshida et al., 2017). The current standard of care dictates a formulaic application of low tidal volumes to reduce overdistension and positive end-expiratory pressure to maintain patency. This approach reduces VILI but does not prevent it in all cases and is not personalized (Network, 2000; Grasso et al., 2007; Khemani et al., 2018). While such protocols have provided measurable improvements in outcomes, the formulaic approach could potentially be improved through personalization of individual respiratory mechanics and VD (Bein et al., 2013).

Modern mechanical ventilators produce data in the form of time-dependent pressure, volume, and flow waveforms that contain a wealth of information about pulmonary physiology, patient-ventilator interactions, and ventilator settings. These data can be used to troubleshoot and optimize mechanical ventilation (Corona and Aumann, 2011; Mellema, 2013). However, ventilator waveforms are typically analyzed heuristically by visual inspection and, therefore, the outcome of such an analysis is limited by individual expertise and experience (Corona and Aumann, 2011; Mellema, 2013). A quantitative interpretation of these complex signals could increase diagnostic accuracy and repeatability while facilitating the application of personalized lung-protective ventilation. One simple example of waveform quantification that is currently used in clinical care is the driving pressure, which serves as a readout of both patient condition and ventilator settings (Amato et al., 2015). In the current study, we seek to develop a model that can systematically mathematize the pathophysiologic knowledge clinicians use to interpret lung conditions from ventilator waveform data as well as knowledge about the processes governed by the ventilator.

The analysis we present herein is a departure from traditional modeling methods that link measured pressures and flows through physiologically-based parameters, such as the well-recognized single-compartment model that lumps the spatially heterogeneous lung mechanical properties into single values of

resistance and compliance (Chiew et al., 2011; Hamlington et al., 2016; Mori, 2016; Mellenthin et al., 2019). In the traditional models, the entirety of the pressure and volume dynamics emerge from the hypothesized physiological mechanics. Due to this straightforward formulation, the single-compartment model is computationally efficient but often not able to reproduce all of the features in waveform data, such as patient-ventilator interaction. This is because the model lacks the complexity to allow such complex dynamics to emerge. Given the complexity of patient-ventilator interactions and pathophysiology present in real human ventilator data, it is unlikely that a two-parameter model that does not incorporate ventilator information will be capable of representing the information that a clinician may want about lung state and pathophysiology. On the other hand, more complicated formulations, including multi-compartment models, use many states and redundant parameters that cannot be uniquely estimated, causing identifiability problems where there is no unique solution, or more often no convergent solution for parameter values. As such, those models require expensive data to estimate that are not currently available for human subjects, and require substantial computational resources. Even then, complex multi-compartment models might not produce all the relevant features present in the pressure and volume waveform data (Rees et al., 2006; Bates, 2009; Reynolds et al., 2010; Molkov et al., 2014, 2017; Roth et al., 2017; Nguyen et al., 2014; Serov et al., 2016; Ellwein Fix et al., 2018). Because of these limitations, both types of models might have a limited use in clinical settings, as the model needs to be useful for a clinician and estimable in real time.

Our approach offers the potential to overcome these limitations and provides both identifiability and fidelity by using mathematical models with interpretable parameters to recapitulate pressure and volume signals. This high fidelity is due, in part, to the limited dependence between the pressure and volume models. The relationship between components of the pressure and volume waveforms are then used to define specific physiologic features, just as the quasi-static compliance is defined from the observed ratio of tidal volume and driving pressure.

Human ventilator waveform data represent several generating processes, lung physiology, ventilator mechanics, interventions, patient-ventilator interactions, and health care process model effects (Hripcak and Albers, 2013b; Rossetti et al., 2021). In general, physiological models alone might be missing substantial contributing sources within the data. There are many potential approaches to manage this problem. One approach would be to include models for the lungs and the ventilator to capture the mechanics of the ventilator, the lungs, and their coupled interaction. Here, instead, we are incorporating both lung and health care process model (ventilator) effects into a single unified model with targeted features captured by lumped parameters. Our model is not a mechanistic model but it is not built arbitrarily either. It is built constructively starting with a lung waveform without pathophysiology or health care processes effects (e.g., the ventilator). We added in limited, e.g., compared to a neural network or other nonlinear regression model, flexibility to the model according to features that the team deemed connected to pathophysiology or health care process model effects. The model

parameters are not like Fourier components that are active during the entire breath, but rather are time-limited breath deformations that are hypothesized to relate to particular types of damage, damage inducing phenomena, and ventilator interactions and effects. It is in this way that the model is constructively anchored to physiology and health care process effects.

Therefore, in this manuscript, our objective is to build a model that takes as baseline “healthy” breaths, and then adds terms that correspond to deviations from healthy breaths whose hypothesized sources include VILI, VD, and pathophysiological features of ventilator waveforms. By estimating the model, we identify the presence and severity of deviations from normal in a way that has a physiologically-based hypothesis attached to it. In essence, this is a proof-in-principle model development manuscript with underlying constraints such that the model could potentially be of use with real clinical data. In future studies, we will tie these phenotypes to lung injury severity, VD, and the pathogenesis of VILI. We anticipate that this approach will eventually find applications in real-time clinical readouts of ventilation safety, long-term monitoring to detect changes in patient condition, and as a quantitative outcome measure for clinical trials.

In the current proof-in-principle study, our team identifies clinically important features in typical volume and pressure waveform data. We then define the models for volume and pressure waveforms as the sum of a set of terms through which we modularly capture physiologically relevant features. The pressure and volume models are coupled via the respiratory rate. This approach allows independent modeling of the waveform components so that clinical, physiologic, and ventilator-based knowledge can be used to constrain the model. We named this model the damage-informed lung-ventilator (DILV) as it contains information about both lung physiology and ventilator dynamics. To demonstrate the model’s flexibility, the volume and pressure models are qualitatively validated in a simulation study where we show various relevant features that are commonly observed in health and disease. We then identify the parameters that may correspond to interpretable pathophysiology by using the DILV model to generate pressure-volume data and qualitatively assessing the effects of parameter changes. Finally, in a quantitative verification, we demonstrate that the model can accurately and uniquely represent laboratory and clinical ventilator data, which includes mouse model and human-intensive care unit (ICU) ventilator data in the absence and presence of VD (Sottile et al., 2018a,b). Through a comprehensive comparison between the DILV model and the single-compartment model, we demonstrate that our approach can accurately determine lung compliance as a baseline evaluation. Temporal changes in the model parameters are compared to other assessments of injury severity and qualitative features of the pressure and volume waveforms.

## MATERIALS AND METHODS

Mechanical ventilation is characterized by three measured state variables which vary over time: volume, pressure and flow.

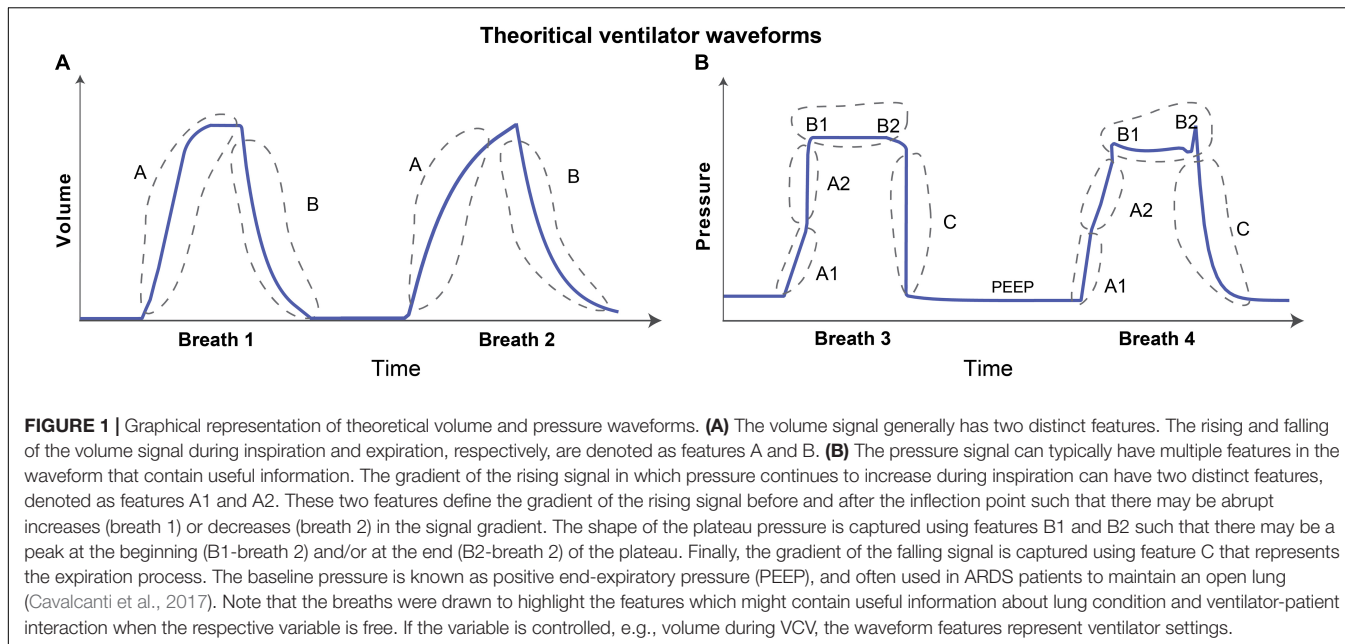
These time-dependent signals have diverse features arising from pulmonary physiology, the ventilator, and health care process effects such as clinical interventions, and patient-ventilator interaction (Albers and Hripcak, 2010; Hripcak and Albers, 2013a,b). The flow is the time-derivative of volume and so the volume variable contains the same information about the underlying lung mechanics but in a different representation (Bates, 2009). In this study, we focused on two state variables, volume and pressure.

In the simplest ventilation modes, one variable is primarily controlled by the ventilator, e.g., pressure or volume, while the other variable, e.g., volume or pressure, is free to vary, referred to as pressure-controlled ventilation (PCV) or volume-controlled (VCV), respectively. In this case, only the “free” variable contains direct information about the respiratory mechanics of the patient (Tobin, 2001; Bates, 2009). Moreover, in some models there is a rigid coupling between the controlled and free states that often limits the model flexibility, precluding the model from reproducing some features that are present in the clinical data. For example, the single-compartment model performs a linear transformation between pressure and volume variables due to the fixed coupling defined as the sum of linear resistive and elastic contributions (Bates, 2009; Smith et al., 2015; Hamlington et al., 2016). We, therefore, do not explicitly couple the controlled (also known as an independent) and free (also known as a dependent) variables such that the volume and pressure models will be independent of one another. Modern clinical ventilators also have an expansive set of other modes, the most notable of which are the patient-triggered modes where the ventilator’s action is triggered by patients such as inspiratory effort. These modes can be very lung-protective, but they can also lead to complex forms of VD that are difficult to model. Patient-triggered modes are the most commonly used modes for humans unless the human is given neuromuscular blockades (Sottile et al., 2018b).

## Identifying Important Features in the Volume and Pressure Waveform

The volume waveform can have two characteristic features as shown schematically in **Figure 1A**. These features might reflect lung condition when volume is the free variable such as in PCV, otherwise these may be controlled via ventilator (Corona and Aumann, 2011; Mellema, 2013). The first feature is the inspiration, denoted as A in **Figure 1A**, which continues until the amount of gas delivered in that breath is reached (the tidal volume). The pressure and lung elastic recoil are at equilibrium. The second feature is expiration, denoted as B in **Figure 1A**. Depending on the ventilator settings and lung condition, the gradient of the rising and falling signals can vary across patients and in the same patient over time. Therefore, the model must be able to represent these features independently. Accordingly, the gradients of inspiration and expiration of volume are features that are variable and estimable in the volume model.

The characteristic shape of the pressure waveform can vary more dramatically than the volume waveform as shown in the hand drawn **Figure 1B**. When pressure is a free variable, such as in VCV, the pressure waveform has several important features



that convey information about lung condition and ventilator-patient interaction. Based on observation of a large number of recorded breaths, we identified five important features in the pressure waveform. Features A1 and A2 in **Figure 1B** determine the gradient of the inspiration. The time-varying graph of inspiration can have two distinct modes where the gradient of the signal may increase (**Figure 1B**, breath 1) or decrease (**Figure 1B**, breath 2) during inspiration. These features are hypothesized to correspond to the volume-dependent decrease in lung compliance (breath 1) or an increase in compliance due to recruitment (breath 2) (Smith et al., 2015; Hamlington et al., 2016). Note that this interpretation is only valid if the flow rate is constant during inspiration (Grasso et al., 2004).

Features B1 and B2 (**Figure 1B**) are related to the shape of the waveform at the start and end of the plateau pressure, which is a period of constant pressure. There may be peaks at the beginning (B1) and/or at the end (B2) of the plateau pressure, which are hypothesized to correspond to inspiratory flow resistance and patient effort, respectively (Bates, 2009; Mellema, 2013). Feature C in **Figure 1B** corresponds to the gradient of expiration. We also model the constant baseline pressure, known as the positive end-expiratory pressure (PEEP), because it is a key independent variable in ARDS management (Guerin, 2011; Cavalcanti et al., 2017). Note that in hybrid ventilation modes, there may be scenarios where both pressure and volume variables are partially controlled and so, in those cases, both the waveforms can be confounded in additionally complex ways and would require more nuanced interpretation.

## Constructing the Damage-Informed Lung Ventilator Model

Once we define the physiological and ventilation-related relevant features in the waveform data, we formulate the model for volume and pressure signals. During this process, we have chosen

minimal number of parameters while ensuring that the model should have the ability to address the deep complexity present in the waveform data due to complex pathophysiology and patient-ventilator interactions. Additionally, the parameters have little overlap as they are not active at the same time within a given breath, and many of the parameters control only specific aspects of a given deformation such as a peak value. In this way, while we add parameters, they act locally along a breath and are tied to a deformation shape and timing that is hypothesized to be related to pathophysiology.

### Construction of the Volume Model

Irrespective of the state variable, the models have periodic dynamics with a frequency defined by the respiratory rate (breaths/min) that should be the same in pressure and volume waveform models. In addition to this constraint, the volume model has two additional features, the rate of inspiration and expiration (A and B in **Figure 1A**, respectively). Volume model development begins by modeling the respiratory rate with a sinusoidal function ( $f_{s1}$ ):

$$f_{s1} = \sin(2\pi\theta t - \phi_1) - b_1. \quad (1)$$

Here, the respiratory frequency (breaths/s) is set by  $\theta$  and  $t$  represents time in seconds while parameter  $\phi_1$  allows to control the starting point in the respiratory cycle. To control the rate of inspiration or expiration while maintaining the periodicity, we create a periodic rectangular waveform function  $f_{b1}$  by combining the sinusoidal function with hyperbolic tangent function:

$$f_{b1} = \frac{1}{2} \{\tanh(a_1 f_{s1}) + 1\}. \quad (2)$$

To control the smoothness of the rectangular waveform, we added a smoothing parameter  $a_1$ . The other terms (1/2, +1)

are added to generate a rectangular waveform that has a zero-base value and unit amplitude. To control the duty cycle of the rectangular waveform that sets inspiratory:expiratory (I:E) ratio, we used parameter  $b_1$  such that the zero value of  $b_1$  corresponds to 1:1 I:E ratio. **Figure 1A** shows additional model features: the rate of inspiration (A) and expiration (B). To represent these rates independently, we define the volume ( $V$ ) using the rectangular waveform as a base waveform:

$$V = A_v (f_{v1} + f_{v2}), \quad (3)$$

where  $f_{v1}$  term produces the inspiration part of the volume signal (feature A):

$$f_{v1}(i+1) = \left\{ \frac{1}{\beta_1} f_{b1}(i+1) + \left(1 - \frac{1}{\beta_1}\right) f_{v1}(i) \right\}; \quad i = 1 : n, \quad (4)$$

$$f_{v1} = [f_{v1}(1) \ f_{v1}(2) \dots \ f_{v1}(i) \dots \ f_{v1}(n)] \ \frac{f_{b1}}{\max(f_{v1})}, \quad (4)$$

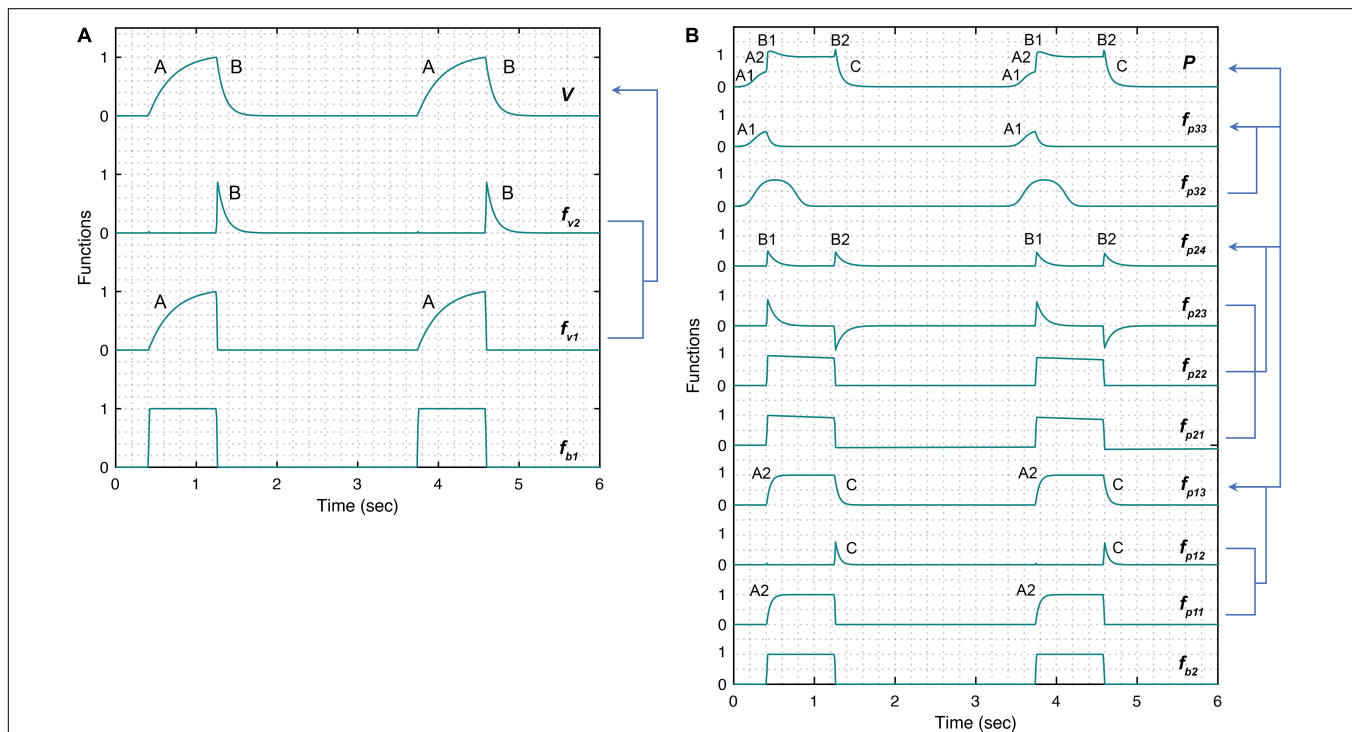


**FIGURE 2 |** Simulated response of various terms that make up the damage-informed volume ( $V$ ) and pressure model ( $P$ ). **(A)** A periodic rectangular waveform  $f_{b1}$  is used to create terms  $f_{v1}$  and  $f_{v2}$  through which the gradient of the rising (feature A) and falling (feature B) signals in the volume waveform are controlled, respectively. Equations 1–5 were used to simulate the response within each term with parameter values  $\theta = 0.3$ ,  $a_1 = 200$ ,  $b_1 = 0.7$ ,  $\phi_1 = 0$ ,  $\beta_1 = 30$ ,  $\beta_2 = 10$ , and  $A_v = 1$ . **(B)** A periodic rectangular waveform ( $f_{b2}$ ) serves as a basis of the pressure model. The overall shape of the pressure waveform, which defines the gradient of the inspiration and expiration signals, is formed using  $f_{p13}$  comprised of the rising signal of  $f_{p11}$  (A2) and falling signal of  $f_{p12}$  (C). The shape of the plateau pressure is defined by  $f_{p24}$ , where the output of  $f_{b2}$  is processed via  $f_{p21}$ ,  $f_{p22}$ , and  $f_{p23}$  to produce peaks at the beginning (B1) and end (B2) of the plateau pressure. The shape of the rising signal at low volume (A1) is defined by  $f_{p31}$ , where a short pulse is produced via  $f_{p31}$  and reshaped via  $f_{p32}$ . Note that the amplitude terms  $A_{p1}$ ,  $A_{p2}$ , and  $A_{p3}$  control the amplitude of  $f_{p13}$ ,  $f_{p24}$ , and  $f_{p33}$ , respectively. Equations 6–18 were used to simulate the response of each term with parameter values  $\theta = 0.3$ ,  $a_2 = 200$ ,  $b_2 = 0.7$ ,  $\phi_2 = 0$ ,  $a_3 = 10$ ,  $b_3 = 0.9$ ,  $\phi_3 = -0.6$ ,  $\beta_3 = \beta_4 = 5$ ,  $\beta_5 = 1.001$ ,  $\beta_6 = 1.1111$ ,  $A_{p1} = 1$ ,  $A_{p2} = 0.5$ ,  $A_{p3} = 0.5$ , and  $A_{p4} = 0$ . Note that the model variability shown here is independent of the ventilator mode.

depicted in **Figure 1B**. Features A1 and A2 capture the gradient of the rising signal during inspiration at low (A1) and high (A2) volume and might be correlated with lung compliance. Features B1 and B2 capture the shape of the peaks at the beginning (B1) and end (B2) of the plateau pressure and might reflect changes in inspiratory flow resistance and patient effort, respectively. Finally, feature C captures the rate of change of the pressure during expiration. To build a model that can capture all these features and be able to estimate parameters reliably and uniquely, we used a modular approach to build the components of the pressure model where each component is controlled by set parameters that form those components.

The pressure model construction begins like the volume model, with a sinusoid. Because volume and pressure are coupled through their period (respiratory rate), we enforce this constraint by requiring that both models have the same respiratory frequency ( $\theta$ ) in their base periodic sinusoid:

$$f_{s2} = \sin(2\pi\theta t - \phi_2) - b_2. \quad (6)$$

Because the pressure may lag or lead the volume depending on the ventilator mode, we include a phase shift term,  $\phi_2$  in the sinusoid. To account for variations in the duty cycle of the rectangular waveform, we added the parameter  $b_2$  that defines the I:E ratio. We then create a rectangular waveform  $f_{b2}$  as we did for the volume model using the hyperbolic tangent:

$$f_{b2} = \frac{1}{2} \{ \tanh(a_2 f_{s2}) + 1 \}. \quad (7)$$

The smoothness of the rectangular waveform is controlled via the parameter  $a_2$ . The five key features in pressure are represented with three additional terms: (i)  $f_{p13}$  defines the rates of pressure change during inspiration and expiration, (ii)  $f_{p24}$  determines the peaks at the beginning and end of the pressure plateau, and (iii)  $f_{p33}$  specifies the gradient of the initial rising signal during inspiration, leaving us with the full the pressure model (P):

$$P = f_{p13} + f_{p24} + f_{p33} + A_{p4}. \quad (8)$$

The constant parameter  $A_{p4}$  corresponds to the baseline pressure value (PEEP). The rates of pressure change during inspiration and expiration (see A2 and C in **Figure 1B**, respectively) are:

$$f_{p13} = A_{p1} (f_{p11} + f_{p12}), \quad (9)$$

where  $f_{p11}$  term produces the rising part of the pressure signal:

$$f_{p11}(i+1) = \left\{ \frac{1}{\beta_3} f_{b2}(i+1) + \left(1 - \frac{1}{\beta_3}\right) f_{p11}(i) \right\}; \quad i = 1 : n, \quad (10)$$

$$f_{p11} = [f_{p11}(1) \ f_{p11}(2) \dots f_{p11}(i) \dots f_{p11}(n)] \frac{f_{b2}}{\max(f_{p11})}, \quad (10)$$

and  $f_{p12}$  term produces the falling part of the pressure signal:

$$f_{p12}(i+1) = \left\{ \frac{1}{\beta_4} f_{b2}(i+1) + \left(1 - \frac{1}{\beta_4}\right) f_{p12}(i) \right\}; \quad i = 1 : n, \quad (11)$$

$$f_{p12} = [f_{p12}(1) \ f_{p12}(2) \dots f_{p12}(i) \dots f_{p12}(n)] \frac{f_{b2}}{\max(f_{p12})}. \quad (11)$$

Here,  $\beta_3$  and  $\beta_4$  control the gradient during inspiration and expiration, respectively. The next set of features, the peaks at the beginning and end of plateau pressure (B1 and B2 in **Figure 1B**), are represented by:

$$f_{p24} = A_{p2} \frac{f_{p23}}{\max(f_{p23})}, \quad (12)$$

where  $f_{p21}$  and  $f_{p22}$  terms create the initial shape of peaks at the plateau pressure:

$$f_{p21}(i+1) = \frac{1}{\beta_5} \{ f_{p21}(i) + \{ f_{b2}(i+1) - f_{b2}(i) \} \}; \quad i = 1 : n, \quad (13)$$

$$f_{p21} = [f_{p21}(1) \ f_{p21}(2) \dots f_{p21}(i) \dots f_{p21}(n)], \quad (13)$$

$$f_{p22} = f_{p21} f_{b2}, \quad (14)$$

and  $f_{p23}$  term further reshapes both the peaks:

$$f_{p23}(i+1) = \frac{1}{\beta_6} \{ f_{p23}(i) + \{ f_{p22}(i+1) - f_{p22}(i) \} \}; \quad i = 1 : n, \quad (15)$$

$$f_{p23} = \text{abs}([f_{p23}(1) \ f_{p23}(2) \dots f_{p23}(i) \dots f_{p23}(n)]). \quad (15)$$

The parameters  $\beta_5$  and  $\beta_6$  control the shape of both the peaks, which are present at the plateau pressure. Finally, the gradient of the initial rate of inspiration (**Figure 1B**, A1) is modeled by:

$$f_{p33} = A_{p3} \frac{f_{p32} \{ 1 - (f_{p11} + f_{p12}) \}}{\max[f_{p32} \{ 1 - (f_{p11} + f_{p12}) \} ]}, \quad (16)$$

where a short pulse is produced via  $f_{p31}$ :

$$f_{p31} = \sin(2\pi\theta t - \phi_3) - b_3, \quad (17)$$

and reshaped via  $f_{p32}$  term:

$$f_{p32} = \frac{1}{2} \{ \tanh(a_3 f_{p31}) + 1 \}. \quad (18)$$

The position, shape and gradient of the rising signal, produced by  $f_{p33}$  term are controlled using the parameters  $\phi_3$ ,  $b_3$  and  $a_3$ , respectively. **Figure 2B** shows the pressure waveform and the constitutive terms added through Eqs 6–18. The pressure waveform (top plot) composed of the three terms  $f_{p13}$ ,  $f_{p24}$ , and  $f_{p33}$  that capture the gradient of the inspiration (A2) and expiration signals (C), the shape of the plateau pressure (B1 and B2), and the shape of the rising signal at low volume (A1), respectively.

## Mouse Mechanical Ventilation Experiments

Three 8 to 10-week-old female BALB/c mice (Jackson Laboratories, Bar Harbor, ME, United States) were studied under University of Colorado, Anschutz Medical Campus Institutional Animal Care and used Committee (IACUC)-approved protocol (#00230). The mice weighed 18.6, 19.1, and 19.9 g. Anesthesia was induced with an intraperitoneal (IP) injection of 100 mg/kg Ketamine and 16 mg/kg Xylazine, a tracheostomy was performed with a blunted 18 ga metal cannula, and ventilation was started on the flexiVent small animal ventilator (SCIREQ, Montreal, QC, Canada). Anesthesia was maintained with 50 mg/kg Ketamine or 50 mg/kg Ketamine with 8 mg/kg Xylazine at 30 min intervals along with 50  $\mu$ L IP 5% dextrose lactated Ringer's solution. Heart rate was monitored via electrocardiogram.

Baseline ventilation, consisting of a tidal volume ( $V_t$ ) = 6 ml/kg, PEEP = 3 cmH<sub>2</sub>O, and respiratory rate (RR) = 250 breaths/min, was applied for a 10 min stabilization period with recruitment maneuvers at 3 min intervals. Pressure and volume were recorded with a custom flowmeter based on our previously published design (Jawde et al., 2018). Four types of ventilation were recorded for analysis: (1) VCV-PEEP0, consisting the baseline ventilation with PEEP = 0 cmH<sub>2</sub>O, (2) VCV-PEEP12 that was the baseline ventilation with PEEP = 12 cmH<sub>2</sub>O, (3) HighPressure-PEEP0 that consisted of a inspiratory pressure (Pplat) = 35 cmH<sub>2</sub>O and PEEP = 0 cmH<sub>2</sub>O with RR = 60 breaths/min, and (4) PCV-PEEP0 with Pplat = 10 and PEEP = 0 cmH<sub>2</sub>O with RR = 70 breaths/min. After the initial measurements of the healthy lung, lung injury was induced with a 0.15 ml lavage with warm saline (Mellenthin et al., 2019). This fluid was pushed into the lung with an additional 0.3 ml air, and suction was applied to the tracheal cannula with an approximate return of 0.05 ml. The mouse was then ventilated for 10 mins with the HighPressure-PEEP0 settings. The sequence of four measurement ventilation patterns (above) was repeated, then the mouse received 0.8 mg/kg IP pancuronium bromide to suppress respiratory efforts, and the measurements were repeated again.

## Human Data Collection

Between June 2014 and January 2017, 140 adult patients admitted to the University of Colorado Hospital medical intensive care unit (MICU) at risk for or with ARDS and requiring mechanical ventilation were enrolled within 12 h of intubation (Wheeler and Bernard, 2007). At risk patients were defined as intubated patients with hypoxemia and a mechanism of lung injury known to cause ARDS, who had not yet met chest X-ray or oxygenation criteria for ARDS. To facilitate the capture of continuous ventilator data, only patients ventilated with a Hamilton G5 ventilator were included. Patients requiring mechanical ventilation only for asthma, COPD, heart failure, or airway protection were excluded. Additionally, patients less than 18 years of age, pregnant, or imprisoned were excluded. The University of Colorado Hospital utilizes a ventilator protocol that incorporated the ARDS network low tidal volume protocol with the low PEEP titration table. The Colorado Multiple Institutional Review Board approved this study and waived the need for informed consent.

Baseline patient information including age, gender, height, and initial P/F ratio were collected. Human patient data shown in **Figures 6A–C** belong to a 62 years old female with an initial P/F 70, height 165 cm, and weight 127 kg. The data shown in **Figures 6D–F** belongs to a 47 years old male, initial P/F 230, height 177 cm, and weight 96.9 kg. Continuous ventilator data were collected using a laptop connected to the ventilator and using Hamilton Data Logger software (Hamilton, v5.0, 2011) to obtain pressure, flow, and volume measurements. Additionally, the DataLogger software allowed collection of ventilator mode and ventilator settings based on mode [i.e.: set tidal, respiratory rate, PEEP, and fraction inspired oxygen (FiO<sub>2</sub>)]. Data were collected until extubation or for up to 7 days per patient.

## Parameter Estimation Methodology

The damage-informed lung ventilator model is a complex model and we estimate its parameters for mouse and human clinical ventilator data. In clinical situations, the patient data are variable and often nonstationary because of interventions, patient-ventilator interactions, changes in health, etc., leading to complex parameter estimation issues. Moreover, the model we develop here is not likely to be structurally identifiable (Westwick and Kearney, 2003; Schoukens et al., 2016; Albers et al., 2019c). However, formally computing identifiability properties here is subtle because many parameters in the model functionally affect only part of the breath. This feature helps facilitate the convergence of parameter estimates and potentially leads to the uniqueness of those estimates, although because the DILV model is neither linear nor convex, there is no guarantee of unique global optima and no way of guaranteeing that the optimal solution we compute is a, or the, global optimum. Nevertheless, this feature—parameters being active at different times during a breath—also makes formal structural identifiability calculations complex to compute. These complexities force us to address four issues, (1) computational estimation methodology, (2) management of parameter identifiability issues and parameter selection methods, (3) uncertainty quantification, and (4) estimation evaluation methodology.

## Computational Estimation Methodology

Our needs require an estimation methodology that allows us to estimate states and parameters of the model effectively and the respective uncertainties in the estimated parameters. While stochastic methods, e.g., Markov Chain Monte Carlo (MCMC) (Gelman et al., 2013), might guarantee to find global minima and quantifying uncertainty in the estimated parameters values, they are generally quite slow. On the other hand, deterministic methods, e.g., Nelder-Mead optimization (Nelder and Mead, 1965), are substantially faster and by choosing many initial conditions, we are still able to quantify the uncertainty of a solution. In particular, here we infer parameters with a standard class of deterministic, multivariate, constrained nonlinear optimization methods, interior-point methods (Bertsimas and Tsitsiklis, 1997; Nocedal, 2006), a choice that is not critical among constrained, nonlinear optimization algorithms. As such, we focus on a smoothing task that employs deterministic nonlinear optimization methods that work well with careful parameter selection and constraints and can be used to quantify uncertainty.

## Management of Parameter Identifiability and Parameter Selection Methods

Irrespective of the estimation methodology, identifiability failure—non-uniqueness of non-convergence of solutions—can occur. In particular, the DILV model is likely not identifiable. To mitigate this problem, we use three different approaches to minimize impacts of identifiability failures while estimating parameters for a given waveform data. First, the model was constructed such that each parameter in the model contributes to the specific feature in the volume and pressure curves, allowing the parameter to be estimated relative to the specific, time-limited feature by definition. Second, we constrain the ranges of all parameters to lie within physically possible values. And third, we do not estimate every parameter in all circumstances but rather limit parameters estimated to those relevant for a given setting and fix many low-impact, low-sensitivity parameters (Law et al., 2015; Asch et al., 2016; Albers et al., 2019b).

In more detail, the DILV model includes two state variables, volume and pressure with one overlapping parameter, the frequency of the breath ( $\theta$ ). The volume model has six parameters ( $a_1$ ,  $b_1$ ,  $\phi_1$ ,  $\beta_1$ ,  $\beta_2$ , and  $A_v$ ). The pressure model has fourteen parameters ( $a_2$ ,  $b_2$ ,  $\phi_2$ ,  $a_3$ ,  $b_3$ ,  $\phi_3$ ,  $\beta_3$ ,  $\beta_4$ ,  $\beta_5$ ,  $\beta_6$ ,  $A_{p1}$ ,  $A_{p2}$ ,  $A_{p3}$ , and  $A_{p4}$ ). Many of these parameters can effectively be uniquely estimated because they operate on a particular part of the waveform, e.g., parameters that control the gradient of the rising signal ( $\beta_1$ ,  $\beta_3$ ) and falling signal ( $\beta_2$ ,  $\beta_4$ ) and amplitudes of the waveforms ( $A_v$ ,  $A_{p1}$ ). Nevertheless, there are parameters that are not necessarily uniquely estimable, e.g., parameters that control feature A1 ( $a_3$ ,  $b_3$ ,  $\phi_3$ , and  $A_{p3}$ ) and features B1 and B2 ( $\beta_5$ ,  $\beta_6$ , and  $A_{p2}$ ).

## Uncertainty Quantification

Because we use deterministic optimization methods whose final solution depends on the initialization, we quantify uncertainty by randomly sampling a set optimization initialization for the parameters we estimate from a uniform distribution within a bounded interval (upper and lower bounds) centered around initial values (Smith, 2013; Albers et al., 2019a). The boundaries of the intervals were chosen to exclude parameter variation that was unrealistic. The upper and lower boundaries of the intervals were chosen by computing parameters that provide a qualitative agreement between the model and the measured response. The optimal parameter estimate is then represented as a probability density in a similar way as is created using MCMC, allowing us to understand how informative, unique, and uncertain a given parameter solution set is. Additionally, we have uncertainty for individual breaths—we estimate every breath many times computing an uncertainty in by-breath parameter estimation—and uncertainty due to variation in many breaths over time. This allows us to both resolve and quantify single-breath features, and how those features vary over time, for different breaths, and even between individuals.

## Estimation Evaluation Methodology

The output of this computational method is a *distribution* of optimal solutions. Through this distribution, we understand the robustness of the solution and the uncertainty of the

solution. If the distribution of solutions has multiple modes with similar error then we can conclude that there are multiple plausible solutions. Similarly, if the distribution of solutions is narrow or wide with similar errors, we can conclude that the model either does or does not depend highly on a given parameter. And finally, it is the distribution of parameter solutions that *define the phenotype computed by the model* in the sense that the distribution of parameters explains the by-breath characterization of the patient. We verify a model's ability to represent data by computing the mean squared error between the model computed with parameter values taken as the medians of the optimally computed solution and the data. There is uncertainty in these MSE values too, and if one model has a lower MSE value than another with non-overlapping uncertainty in MSE, we conclude that the model with the lower median MSE more accurately represents the data.

## RESULTS

In this section, we qualitative and quantitative validate the DILV model using numerical simulations and measured data, respectively.

### Qualitative Model Validation, Parametric Descriptions, and Simulated Model Variability

The first step in model validation is the qualitative validation (Jolliffe and Stephenson, 2012) that involves demonstrating the model has enough flexibility to recapitulate the key features that are often seen in clinically collected volume and pressure waveform data. We then identify the parameters that correspond to hypothesized lung physiology by analyzing simulated pressure and volume waveforms.

#### Volume Model Flexibility

The volume model flexibility is demonstrated in **Figure 3** where we vary the rates of inspiration (feature A) and expiration (feature B) through the terms  $f_{v1}$  and  $f_{v2}$ , which are controlled by parameters  $\beta_1$  and  $\beta_2$  (**Figures 3A,B**), respectively. The full variability of terms  $f_{v1}$  and  $f_{v2}$  is shown in **Supplementary Figure 1**. Additionally, the amplitude of the volume waveform is controlled by  $A_v$  (**Figure 3C**), variations in respiratory rate are controlled by  $\theta$  (**Figure 3D**). Finally, the I:E ratio, the starting point of the breath in the breathing cycle and the smoothness of the waveform are set by  $b_1$ ,  $\phi_1$ , and  $a_1$  as shown in **Supplementary Figure 2**, respectively.

#### Pressure Model Flexibility

The pressure model flexibility is demonstrated in **Figure 4** where we vary the five features of the pressure waveform via respective parameters: variation in the rate of change of the pressure before (A1 in **Figure 1B**) and after (A2 in **Figure 1B**) the inflection point during inspiration; the shape of the peaks at the beginning (B1 in **Figure 1B**) and end (B2 in **Figure 1B**) of the plateau pressure; and variation in the rate of change of the pressure during expiration

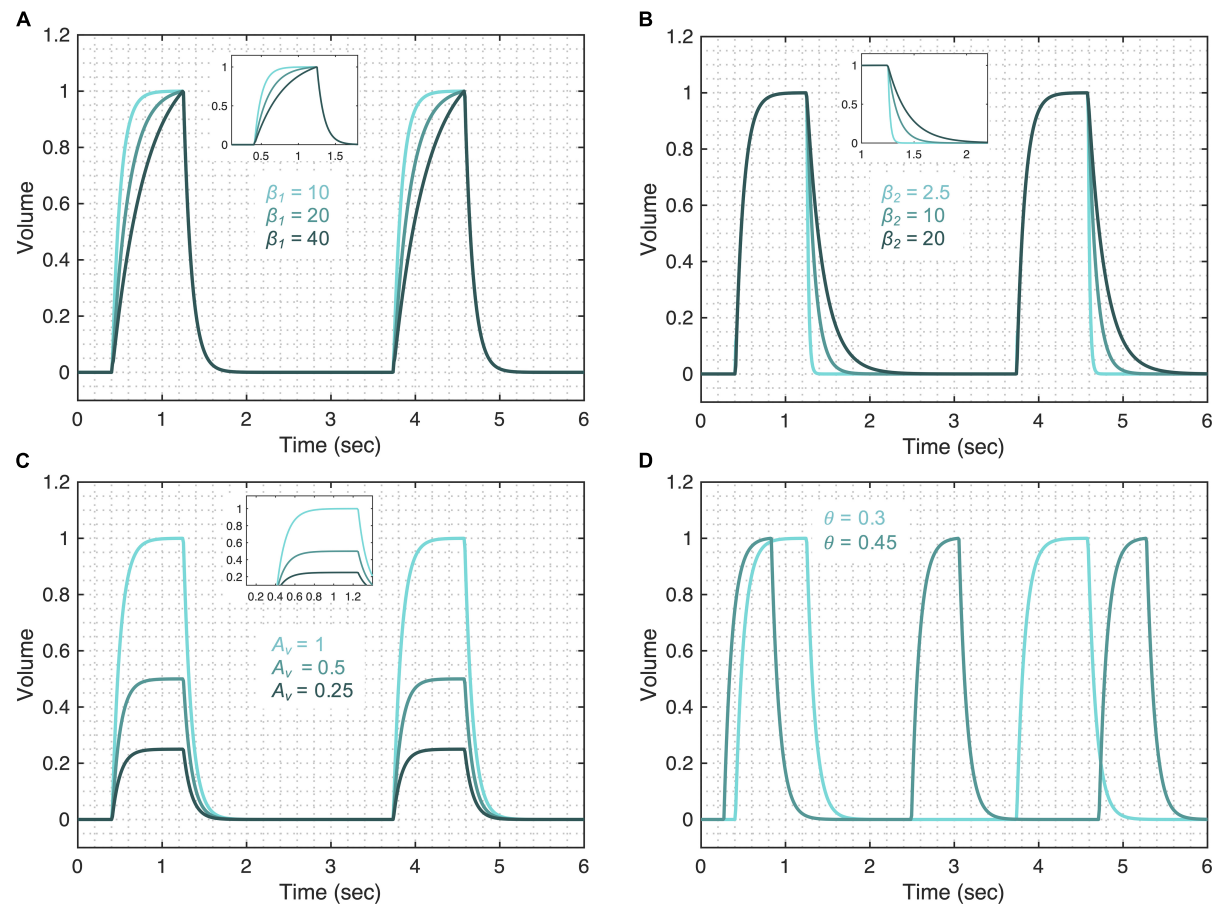


**FIGURE 3 |** Demonstrating the volume model flexibility by varying parameters that alter characteristic features of the volume waveform. The gradient of the rising and falling signals can be altered using the **(A)**  $\beta_1$  and **(B)**  $\beta_2$  parameters, respectively. Increased values of these parameters increase the transient time for the signal to reach the same volume level. **(C)** The amplitude of the waveform can be altered using the parameter  $A_v$ . **(D)** Changes in the respiratory frequency ( $\theta$ ) change the period of the breath. The output of the model ( $V$ ) was calculated using Eqs 1–5 while considering  $\theta = 0.3$ ,  $a_1 = 200$ ,  $b_1 = 0.7$ ,  $\phi_1 = 0$ ,  $\beta_1 = 30$ ,  $\beta_2 = 10$ , and  $A_v = 1$ . The respective variation in the functions that make the volume model is shown in **Supplementary Figure 1** for each case. Note that the model variability shown here is independent of the ventilator mode.

(C in **Figure 1B**). In brief, these features are controlled by the following parameters.

The initial gradient of the pressure during inspiration ( $A_1$ ) is controlled by the  $a_3$  parameter such that higher values of  $a_3$  result in a slower rising signal (**Figure 4A**). The full variation that these terms are capable of is shown in **Supplementary Figure 3**. The shape of the initial gradient signal ( $A_1$ ) before the inflection point can be altered using the  $b_3$  parameter (**Supplementary Figure 4A**) and the amplitude of the initial gradient alteration is controlled by the  $A_{p3}$  parameter (**Supplementary Figure 4B**). By setting  $A_{p3}$  parameter to zero, feature A1 can be removed from the pressure waveforms. The rate of inspiratory pressure after the inflection point ( $A_2$ ) is specified by  $\beta_3$  such that higher values of  $\beta_3$  result in a slower rising signal (**Figure 4B**). The shapes of the peaks at the beginning (B1) and end (B2) of the plateau pressure are controlled by several parameters. The overall shape of the peaks is controlled by the  $\beta_5$  (**Figure 4C**) and the sharpness of these peaks can be further altered by  $\beta_6$  (**Supplementary Figure 4C**). The amplitude of the peaks

is controlled by  $A_{p2}$  (**Supplementary Figure 4D**). By setting  $A_{p2}$  parameter to zero, features B1 and B2 can be turned off. Additional control of features B1 and B2 can be achieved in combination with parameter  $\beta_3$  shown in **Supplementary Figures 4E,F**. The rate of pressure decrease during expiration (C) is specified by  $\beta_4$  such that higher values of  $\beta_4$  result in a slower falling signal (**Figure 4D**). Finally, the amplitude of the plateau pressure can be altered using the  $A_{p1}$  parameter (**Supplementary Figure 4G**). The I:E ratio is defined by the  $b_2$  parameter in the same way that parameter  $b_1$  controls the I:E ratio in the volume model (**Supplementary Figure 2A**). A summary of model parameters is provided in **Table 1**.

### Qualitatively Relating the Model Parameters With the Lung Function Parameters

In order to be able to use the DILV model parameters to infer lung health, it is required that we set up the initial framework

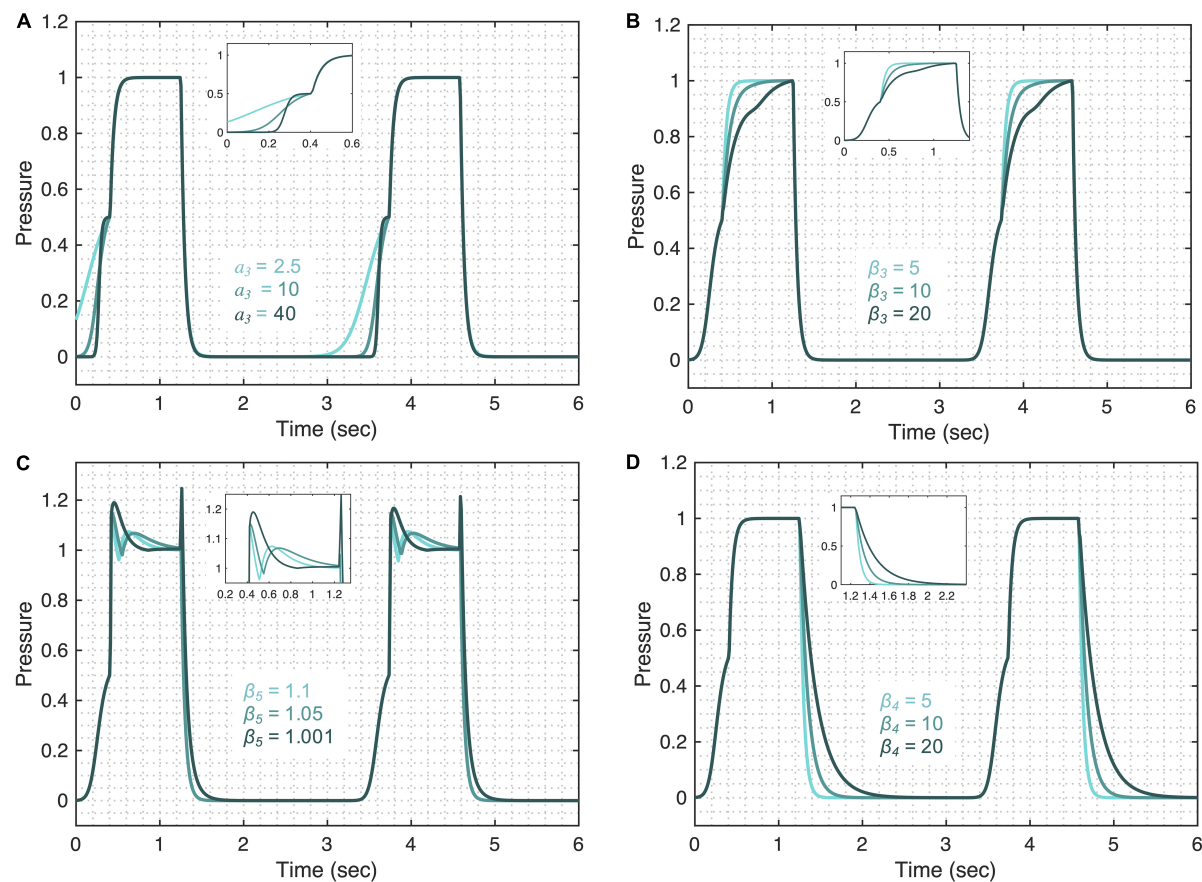


**FIGURE 4 |** Demonstrating the pressure model flexibility by altering relevant features in the pressure waveform. The initial gradient of the pressure signal during inspiration at low volume (feature A1) is controlled by **(A)** the  $a_3$  parameter. **(B)** The gradient of the rising signal after the inflection point (feature A2), is controlled by the  $\beta_3$  parameter. **(C)** The shapes of the peaks at the beginning (feature B1) and at the end (feature B2) of the plateau are regulated by the  $\beta_5$  parameter when  $A_{p4} = 0.5$ . **(D)** The gradient of the falling signal (feature C) during expiration can be modified by the  $\beta_4$  parameter. Equations 6–18 were used to simulate the response of the pressure model while considering  $\theta = 0.3$ ,  $a_2 = 200$ ,  $b_2 = 0.7$ ,  $\phi_2 = 0$ ,  $a_3 = 10$ ,  $b_3 = 0.9$ ,  $\phi_3 = -0.6$ ,  $\beta_3 = \beta_4 = 5$ ,  $\beta_5 = 1.001$ ,  $\beta_6 = 1.1111$ ,  $A_{p1} = 1$ ,  $A_{p2} = 0.5$ ,  $A_{p3} = 0.5$ , and  $A_{p4} = 0$ . The respective variations in the terms that make the pressure model are shown in the **Supplementary Figure 3** for each case. Note that the model variability shown here is independent of the ventilator mode.

to correlate the model parameter with the lung condition, given the model parameters are not physiological parameters but rather chosen to control specific features in the waveform data. On this account, the DILV model is anchored to physiology through variations or deviations from nominal breath waveforms that are hypothesized to relate to lung conditions observed in mechanical ventilation data collected in lab and clinical settings. Throughout the manuscript, we list the proposed physiological interpretations of the parameters – a short description of how the model parameters contribute to the model is provided in **Table 1** – but here we will go into interpretative depth regarding the qualitative correlation between model parameters and the fundamental characteristics of the lung such as compliance and resistance. In this qualitative interpretation, we consider only one variable (volume in PCV and pressure in VCV) while assuming the other waveform does not change breath-to-breath (pressure in PCV and volume in VCV).

We first show how the changes in the volume model parameters can be qualitatively related to changes in lung

compliance and resistance when the volume variable is free. For that, we focus on three model parameters that might have direct physiological meaning:  $\beta_1$ ,  $\beta_2$ , and  $A_v$ . The first parameter,  $\beta_1$  might be inversely correlated with lung compliance as higher values of  $\beta_1$  result in a lower inspiratory flow rate (**Figure 3A** and **Supplementary Figure 5A**). During PCV, the inspiratory flow rate will decrease with reduced compliance or increased resistance. A second parameter,  $\beta_2$ , controls the gradient of expiration and is captured as feature B in **Figure 1A**. Higher values of  $\beta_2$  result in a longer expiration (cf. **Figure 3B** and **Supplementary Figure 5A**) and so  $\beta_2$  is directly proportional to the expiratory time constant, which is the product of resistance and compliance. Finally, parameter  $A_v$  controls the amplitude of the volume waveform and for the same pressure waveform (in PCV) indicates a direct correlation with compliance (**Figure 3C** and **Supplementary Figure 5A**). In VCV, parameter  $A_v$  would present the tidal volume, which is set by the ventilator.

The pressure model has five parameters that may reflect aspects of lung compliance during VCV:  $a_3$ ,  $b_3$ ,  $\beta_3$ ,  $A_{p1}$ , and

**TABLE 1 |** Interpreting damaged-informed lung ventilator model parameters.

Parameter	Model relevance	Physiological relevance (with increased values)
<b>Volume model</b>		
$\theta$	Number of breaths/s. Higher values result in a higher number of breaths/s	–
$a_1$	Smoothness of the square waveform ( $f_{b1}$ ). Higher values result in a sharper transition	–
$b_1$	I:E ratio. Higher values result in smaller inspiration cycle	–
$\Phi_1$	Starting of the inspiration point. Higher value results in a more delayed response	–
$\beta_1$	Gradient of the rising signal. Higher values result in a slower rising signal	Lower compliance and/or higher resistance
$\beta_2$	Gradient of the falling signal. Higher values result in a slower falling signal	Higher expiration time constant
$A_v$	Peak amplitude	Higher overall compliance
<b>Pressure model</b>		
$b_2$	I:E ratio. Higher values result in a smaller inspiration cycle	–
$a_2$	Smoothness of the square waveform. Higher values result in a sharper transition	–
$\Phi_2$	Starting of the $f_{b2}$ function. Higher value results in a more delayed response	–
$a_3, b_3$	Gradient of the pressure signal at low volume. Higher values result in a slower rise	Higher low volume compliance
$\Phi_3$	Starting of the inspiration point. Higher value results in a more delayed response	–
$\beta_3$	Gradient of the rising signal after inflection point. Higher values result in a slower rising signal	Higher high-volume compliance
$\beta_4$	Gradient of the falling signal. Higher values result in a slower falling signal	–
$\beta_5, \beta_6$	Shape of plateau. Higher value means a sharper peak	Associated with ventilator desynchrony
$A_{p1}$	Peak amplitude	Lower high-volume compliance
$A_{p2}$	Amplitude of the peaks at the plateau	–
$A_{p3}$	Higher values increase the amplitude of $f_{p33}$ function	Moves upper inflection point up
$A_{p4}$	Pressure base line value	PEEP

The parameters that are correlated with known measures of lung physiology are in bold.

$A_{p3}$ . The parameter  $a_3$ , which controls feature A1 (Figure 4A), may be directly correlated with low-volume compliance as higher values of  $a_3$  result in slower pressure rise at low volume while maintaining the shape of the gradient (Supplementary Figure 5B). Additionally, parameter  $b_3$  can also be used to control feature A1 (Supplementary Figure 5B) and is directly related to the low-volume compliance. A third parameter,  $\beta_3$  controls the rate of pressure increase above the inspiratory inflection point (A2), and higher values of  $\beta_3$  result in slower pressure increase (Supplementary Figure 5B), indicating  $\beta_3$  might be correlated with high-volume compliance during VCV. A fourth parameter,  $A_{p1}$ , defines the plateau pressure with higher values of  $A_{p1}$  yielding higher plateau pressures (Supplementary Figure 5B), indicating an inverse correlation between  $A_{p1}$  and compliance during VCV. Finally, change in the upper inflection point (UIP) can be directly related to the  $A_{p3}$  parameter such that higher values of  $A_{p3}$  increase the UIP pressure as shown in Supplementary Figure 5B. During PCV, these (and other) parameters may be directly controlled via a ventilator.

It is important to note that these interpretations are qualitative and valid only when a change is observed in one of the variables (volume or pressure) while the other waveform (pressure or volume) is held fixed. In cases where both the volume and pressure waveforms change simultaneously, additional interpretation is needed to establish the relationships between pressure and volume parameters. For example, in the pressure signal, interpretation of feature A2 with respect to A1 will be valid only during the constant flow signal (Grasso et al., 2004). Similarly, when there is a change in the amplitude of volume and pressure simultaneously, we use the  $A_v/A_{p1}$  to assess compliance.

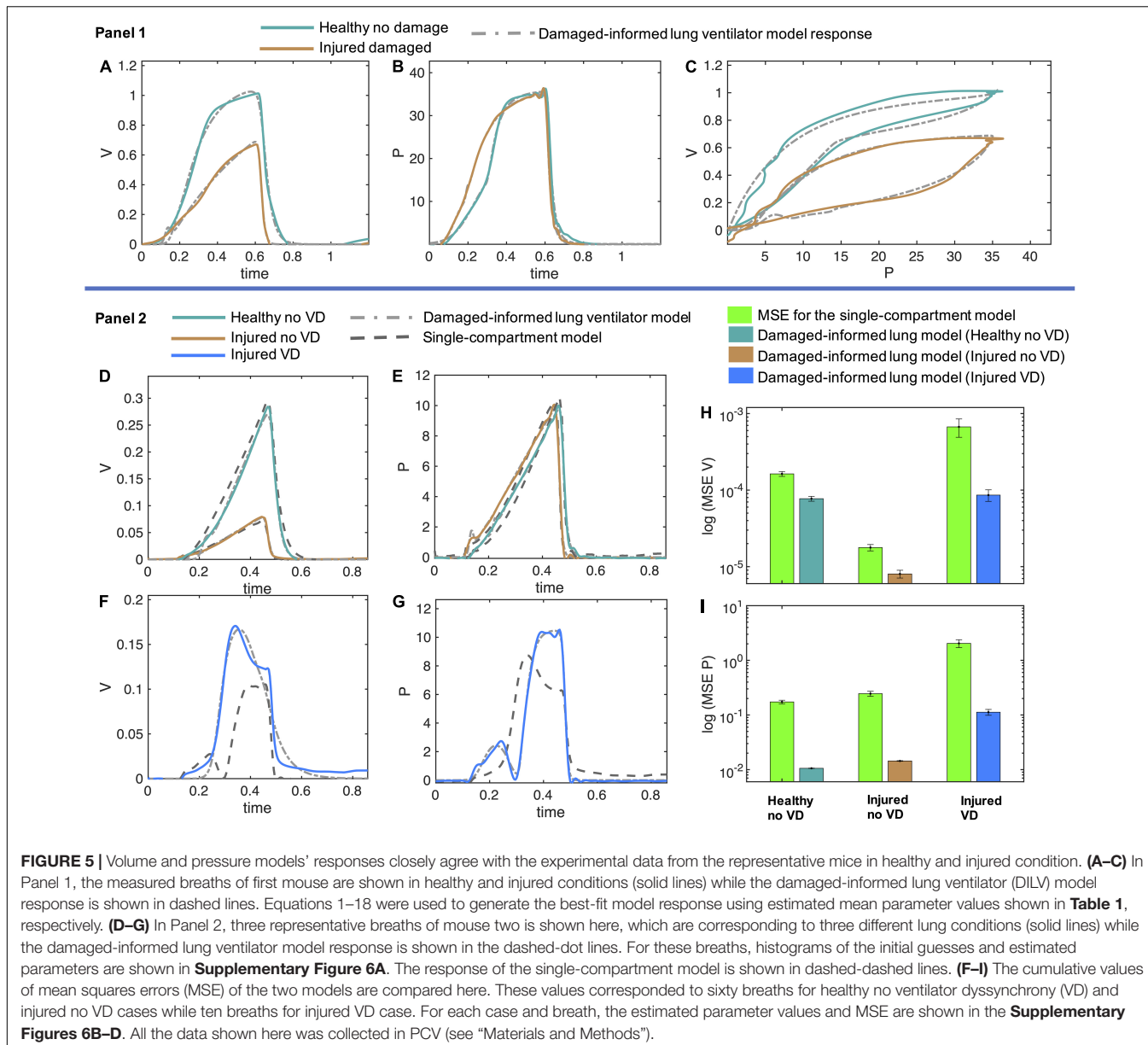
## Damage-Informed Lung Ventilator Model Quantitative Verification for Experimental Mouse Model Ventilator Data

To demonstrate the effectiveness of the DILV model, we now quantitatively validate the model by estimating parameters for data sets corresponding to different phenotypes—e.g., injured versus healthy. We then show that differences in the estimated parameter values reflect different phenotypic states in a manner that is consistent with expected changes due to acute lung injury. Here we consider data from PCV and VCV, in healthy and lung-injured mice, and in the absence and presence of VD.

### In Pressure Controlled Ventilation, the Model Outcomes Align With the Injury Status and Single Compartment Model

Figures 5A,B, panel 1 shows two different pressure-controlled breaths recorded in a healthy mouse (green) and after a lung injury induced by injurious lavage and mechanical ventilation (orange). The pressure-volume loops (Figure 5C) show a reduction in lung compliance and an increase in hysteresis that is characteristic of acute lung injury. The DILV model estimated states (dashed-dot lines) show the same trends. The estimated parameter values and the respective uncertainty for individual breaths are shown in Table 2 with bold indicating physiological relevance.

In the volume model, the injured lung showed a lower inspiratory flow rate, quantified by an increase in  $\beta_1$ , and a faster expiration, quantified by a reduction in both  $\beta_2$  and  $A_v$  than the healthy lung model estimates. Given that the inspiratory



pressures remain unchanged, this suggests a reduction in lung compliance, and the associated decrease in the expiratory time constant (See Table 1).

Physiologic interpretation of the pressure model is limited because of the use of PCV. In this case, the pressure signal is prescribed by the piston ventilator and the observed differences between the healthy and injured lungs are a result of the ventilator control system algorithms. Hence, the respective changes in the parameters' values, such as an increase in parameters  $a_3$  and  $\beta_3$  correspond to the changes in the ventilator dynamics and not in the respiratory mechanics. These results make an important point: it is essential to see the relative change in the parameters that control these features and to synthesize the model-based inference in a holistic fashion, instead of focusing on any one parameter or feature in isolation.

To analyze changes in lung mechanics in a manner that accounts for ventilator settings, we define the lung compliance  $Cd = A_v/A_{p1}$  (Table 2), which is the ratio of volume and pressure model amplitudes. As expected,  $Cd$  decreases with injury. Furthermore,  $Cd$  shows a strong correlation with compliance ( $Cs$ ) calculated with the single-compartment model (Table 2; Mellema, 2013).

#### Damaged-Informed Lung Ventilator Model Accurately Captures Mouse Model Data With Ventilator Dyssynchrony While the Single-Compartment Model Is Unable to Capture This Variability

In the previous section, we demonstrate that the DILV model can accurately estimate a single breath. We did not, however, validate that the model has enough flexibility to account

**TABLE 2 |** Estimated model parameters obtained from the optimization scheme for the results shown in **Figure 5** (Panel 1) and **Figure 6** (human patient 1) correspond to the mouse and human data, respectively.

Parameters	Figure 5 (Panel 1)		Figure 6 (Patient 1)	
	Healthy	Injured	Beginning	Ending
$\theta$	0.66 ± 0.000	0.66 ± 0.000	0.34 ± 0.000	0.35 ± 0.000
$a_1$	9.67 ± 0.385	15.41 ± 0.397	7.51 ± 0.258	7.57 ± 0.282
$b_1$	0.59 ± 0.006	0.53 ± 0.006	0.66 ± 0.000	0.63 ± 0.000
$\Phi_1$	0.09 ± 0.007	-0.01 ± 0.007	0.42 ± 0.003	0.51 ± 0.002
$\beta_1$	<b>112.97 ± 9.733</b>	<b>458.95 ± 8.179</b>	<b>10.96 ± 0.223</b>	<b>12.53 ± 0.240</b>
$\beta_2$	<b>28.35 ± 10.490</b>	<b>10.60 ± 10.590</b>	<b>12.42 ± 0.051</b>	<b>12.64 ± 0.039</b>
$A_v$	<b>1.03 ± 0.006</b>	<b>0.70 ± 0.003</b>	<b>402.61 ± 0.368</b>	<b>337.08 ± 0.531</b>
$a_2$	52.06 ± 1.440	32.11 ± 1.514	27.39 ± 0.118	17.73 ± 0.163
$b_2$	0.80 ± 0.002	0.66 ± 0.001	0.67 ± 0.000	0.66 ± 0.000
$\Phi_2$	0.34 ± 0.002	0.09 ± 0.002	0.35 ± 0.002	0.32 ± 0.001
$a_3$	<b>2.55 ± 0.334</b>	<b>5.11 ± 0.205</b>	<b>7.71 ± 0.183</b>	<b>18.37 ± 0.146</b>
$b_3$	<b>1.00 ± 0.002</b>	<b>0.53 ± 0.003</b>	<b>0.91 ± 0.000</b>	<b>0.90 ± 0.000</b>
$\Phi_3$	0.00 ± 0.002	0.00 ± 0.005	0.15 ± 0.001	0.14 ± 0.001
$\beta_3$	<b>50.00 ± 0.388</b>	<b>100.84 ± 0.262</b>	<b>7.25 ± 0.157</b>	<b>12.88 ± 0.147</b>
$\beta_4$	18.54 ± 0.239	11.93 ± 0.193	1.95 ± 0.121	2.52 ± 0.064
$\beta_5$	-	-	1.0014 ± 0.0001	1.0048 ± 0.0001
$\beta_6$	-	-	1.1262 ± 0.0012	1.0771 ± 0.0055
$A_{p1}$	<b>35.53 ± 0.018</b>	<b>35.02 ± 0.017</b>	<b>16.58 ± 0.018</b>	<b>11.64 ± 0.008</b>
$A_{p2}$	-	-	3.80 ± 0.011	2.48 ± 0.022
$A_{p3}$	<b>14.00 ± 0.081</b>	<b>9.60 ± 0.077</b>	<b>3.90 ± 0.022</b>	<b>4.10 ± 0.016</b>
$A_{p4}$	0.06 ± 0.035	0.00 ± 0.021	19.98 ± 0.011	17.91 ± 0.004
$C_s$	0.030	0.019	26.80	31.40
$C_d$	0.029	0.020	24.28	28.96

The error values were determined using the standard error of the mean for individual breaths. To quantify uncertainty in parameter estimates, each individual breath was estimated 1,000 times. The parameters that are correlated with a known measure of lung physiology are in bold. Here,  $C_s$  and  $C_d$  are lung compliance values extracted by fitting the single-compartment model to data ( $C_s$ ) and from the damaged-informed lung ventilator model ( $C_d$ ) =  $A_v/A_{p1}$ .

for large variations in the waveform data, or that the DILV model can estimate a large number of breaths reliably while maintaining unique and consistent solutions of parameters values for each breath. To show these characteristics, we estimate a large number of breaths for the second mouse in three different lung conditions: (1) healthy breaths without VD, (2) injured breaths without VD, and (3) injured breaths with VD (See “Materials and Methods”). In the 1st and 2nd cases, we selected sixty breaths in a sequence from the random location out of 424 and 128 breaths, respectively. In the 3rd case, we manually selected ten breaths out of 332 breaths that had VD from the data set containing breaths with and without VD. Here, we define VD as any substantial respiratory effort because the flexiVent small animal ventilators do not allow the subject to trigger a breath. A representative breath for each case is shown in **Figures 5D–G**, panel 2 along with the DILV model response at the optimum parameter values, which are listed in **Supplementary Table 1**. Histograms of the initial guesses and estimated parameters are shown in the **Supplementary Figure 6A**. We observed minor variability in most of the estimated parameters values for individual breaths, suggesting that those features are modularly controlled by the respective parameter. We do observe high variability in some parameters ( $a_1$ ,  $\beta_1$ ,  $a_3$ , and  $\beta_3$ ) due to the low sensitivity of the model for those parameters (**Supplementary Figure 6A**).

To demonstrate what is gained by the DILV model we compare it to single-compartment model (Bates, 2009) estimated resistance and compliance to estimate the same breaths for each case (**Figure 5**, panel 2). The single-compartment model has substantially larger estimated mean squares errors (MSE) and these errors increase as the mouse lung condition worsens and in the presence of VD (**Figures 5H,I** and **Supplementary Figures 6B–D**). Consequently, in terms of lung compliance values, the two models’ outcomes closely agree in the healthy lung case but then diverge somewhat for the injured lung and more substantially during VD (**Supplementary Figures 6E–G**). These discrepancies have their root in the limited ability of the single-compartment model to estimate VD (**Figures 5F,G**), errors that are quantified by the MSE between model estimates and data (**Supplementary Figures 6B–D**). Note that the calculated compliance values include the effects of muscle effort, which explain the differences in compliance with and without VD in the same injured mouse.

### In Volume-Controlled Ventilation, the Pressure Model Outcomes Align With the Injury Status and the Single Compartment Model

Above we verified the DILV model using data sets collected during PCV, where the estimated volume model parameters reflected the lung dynamics since the volume was the free variable. We now consider data collected during VCV so that

the estimated pressure model parameters reflect changes in lung condition. Here, we consider variations in PEEP during low tidal volume ventilation (VCV). The pressure model indicates a reduction in compliance in the injured lung as quantified by lower values of parameters  $a_3$ ,  $b_3$ , and  $\beta_3$ , and elevated estimates of  $A_{p1}$  (**Table 1**, **Supplementary Figure 7**, and **Supplementary Table 1**). In contrast to the PCV results shown in **Figure 5**, differences in parameter estimates between healthy and injured lungs in the pressure model were much larger compared to those estimated differences in the volume model. This is expected since the tidal volumes were approximately equal during VCV, and the reduction in compliance is reflected in increased pressure. This effect can be inferred by analyzing the  $A_v/A_{p1}$  ratio showing a reduction in the injured cases at both the PEEP settings (**Supplementary Table 1**). We also note that the healthy lung becomes stiffer at  $\text{PEEP} = 12 \text{ cmH}_2\text{O}$  due to strain stiffening. In contrast, the injured lung becomes more compliant at high PEEP, which our previous studies in this injury model attribute to recruitment (Mellenthin et al., 2019).

## Damage-Informed Lung Ventilator Model Quantitative Verification for Intensive Care Unit Patient-Ventilator Data

The DILV model is intended to be used with both laboratory data and clinical ventilator data where standard models, such as the single-compartment model, cannot recapitulate all of the potentially relevant waveform features. To show the clinical applicability of the DILV model we consider waveform data of two ICU patients, the first—patient 1—includes waveform data without VD and the second—patient 2—has waveform data with VD. For each case, we estimate each individual breath 1,000 times to quantify uncertainty in parameter estimates for each of 263 breaths to quantify uncertainty in parameter estimates across many breaths. These data were recorded near extubation when ARDS had nearly resolved. For both patients, the ventilator was operating in patient-triggered mode, a ventilator mode that is not possible in our mouse ventilators but is commonly used in the ICU.

### Intensive Care Unit Data-Driven Verification in the Absence of Ventilator Dyssynchrony (Patient 1)

For patient 1, we selected a sequence of 130 breaths without VD at a random location out of 1,829 breaths and performed parameters estimation breath by breath. The sequence of breaths starts at  $\text{PEEP} = 20 \text{ cmH}_2\text{O}$  and switches to  $\text{PEEP} = 18 \text{ cmH}_2\text{O}$  at breath number 68. **Figures 6A–C** shows two representative breaths along with the DILV model response at the optimum parameter values (**Table 2**). Histograms of the initial guesses and estimated parameters are shown in the **Supplementary Figure 8A** for the respective breaths. For all the model parameters, we observed unimodal estimated parameter distributions with low variance, suggesting that each parameter controls a specific feature of the waveform. We also estimated each breath using the single-compartment model and substantially higher MSE compared to the DILV model (**Figures 6G,H**). Note that in **Figures 6G–J**, an MSE ratio less

than one indicates that the DILV model produced waveforms that were more similar to the measured data.

Pressure-volume (PV) loops for these cases (**Figure 6C**) suggest that lung compliance is increased by the prescribed change in PEEP. We found that the model-estimated parameters indicate an increase in compliance (the  $A_v/A_{p1}$  ratio) with a reduction in PEEP (**Table 2**). The increased compliance at lower PEEP agrees with the single-compartment model (Bates, 2009) response (**Supplementary Figures 8B,C**) and also the patient outcome (successful extubation). Moreover, a significant increase in parameters  $a_3$  and  $\beta_3$  suggested the same (**Table 2**). The prescribed reduction in PEEP was reflected in a reduction in  $A_{p4}$ .

### Intensive Care Unit Data-Driven Verification in the Presence of Ventilator Dyssynchrony (Patient 2)

In the cases where VD is present a more thorough parameter interpretation is needed to quantify and understand the patient-ventilator interaction. To show this, from patient 2's data we randomly selected 133 breaths out of 3,201 breaths that showed mild to severe flow limited VD. Two representative breaths for this case are shown in **Figures 6D–F** along with the DILV model's estimate of these breaths at the optimum parameter values (**Supplementary Table 1**) and the single compartment model fit. Histograms of the initial guesses and estimated parameters for these breaths are shown in the **Supplementary Figure 9A**.

PV loops for these breaths (**Figure 6F**) suggest that lung compliance is increased prior to extubation compared to earlier in the ICU course. This qualitative observation is supported by the increased  $A_v/A_{p1}$  ratio (**Supplementary Table 1**) that is a measure of compliance. However, it is important to note that this compliance includes the additional effects of VD. To further demonstrate the importance of the DILV model, we compared the DILV model's estimate of the breaths with the single-compartment model (Bates, 2009) estimates for each breath. The single-compartment model estimates of the breaths have substantially higher MSE values for patient 2 compared to patient 1 (**Figures 6G–J**) due to the presence of VD. Accordingly, we expect large errors in the compliance values estimated with the single-compartment model (**Supplementary Figures 9B,C**). These results agree with the fact that the DILV model can estimate the volume and pressure waveform data more accurately, especially when the waveforms have high variability, as in the case of patient 2 with VD.

The mouse data verification showed that the DILV model is able to estimate most of the parameters for individual breaths. It is also important to quantify uncertainty across many breaths and in different patients. Analyzing the variability in the estimated parameters over several breaths might capture the lung condition's heterogeneous nature, including many potentially different and differently damaging breaths that show VD. In the ICU, there are no controlled experiments, and patients simultaneously experience many types and severities of VD, different interventions, heterogeneous injurious insults, etc. As such, we expect to see minor variability in parameter estimates when many breaths of a patient are approximately the same compared to large variability in the parameter estimates when breaths are heterogeneous. For example, we observed a low

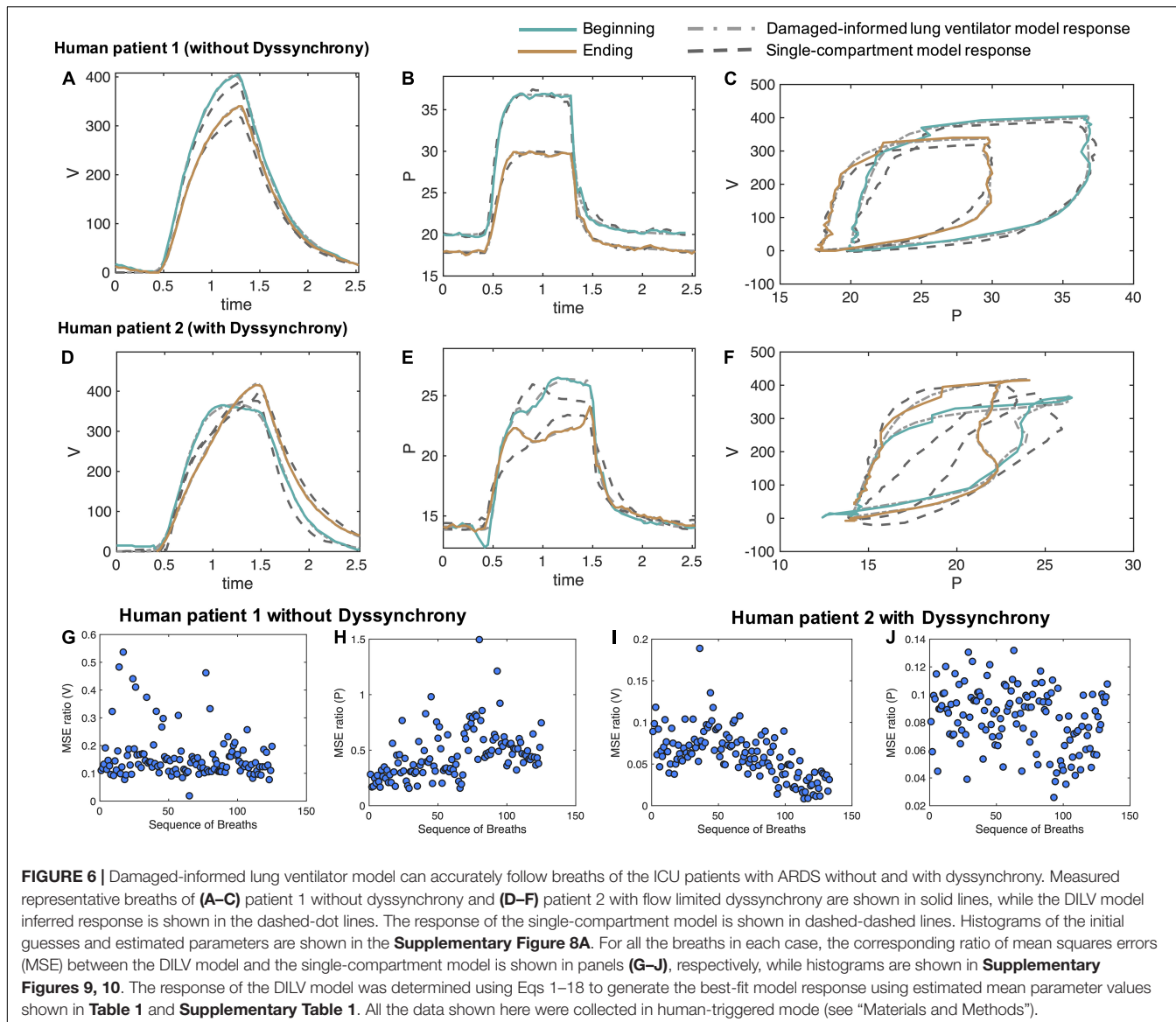


**FIGURE 6 |** Damaged-informed lung ventilator model can accurately follow breaths of the ICU patients with ARDS without and with dyssynchrony. Measured representative breaths of (A–C) patient 1 without dyssynchrony and (D–F) patient 2 with flow limited dyssynchrony are shown in solid lines, while the DILV model inferred response is shown in the dashed-dot lines. The response of the single-compartment model is shown in dashed-dashed lines. Histograms of the initial guesses and estimated parameters are shown in the **Supplementary Figure 8A**. For all the breaths in each case, the corresponding ratio of mean squares errors (MSE) between the DILV model and the single-compartment model is shown in panels (G–J), respectively, while histograms are shown in **Supplementary Figures 9, 10**. The response of the DILV model was determined using Eqs 1–18 to generate the best-fit model response using estimated mean parameter values shown in **Table 1** and **Supplementary Table 1**. All the data shown here were collected in human-triggered mode (see “Materials and Methods”).

variability in all the volume model parameters over several breaths with the exception of  $A_v$  for patient 1, indicating that the volume waveforms' characteristic shape remains the same at different time points except for variations in tidal volume. This contrasts with what we observed for patient 2 where VD drove heterogeneity and substantial deviations from more normal breaths (**Supplementary Figures 10, 11**). More importantly, parameters associated with patient-VD can be used to infer the presence of VD. In patient 2, we observed increases in the  $\beta_5$ ,  $\beta_6$ , and  $A_{p2}$  parameters which align with the visual determination of VD in those breaths (**Supplementary Figures 10, 11**).

Taken together, these results suggest that the DILV model can reproduce a wide variety of waveform data and is capable of extracting hypothesis-driven, clinically-relevant information from the waveforms that might facilitate a systematic interpretation of the dynamics of the injured lung.

## DISCUSSION

In this work, we developed a new damage-informed lung ventilator model that represents pressure and volume waveform data by reconstructing the waveforms from hypothesis-driven modular subcomponents. We then performed a proof-in-principle verification that the model can potentially represent hypothesized damage in humans and mice. The model accurately estimated pressure and volume waveforms data and consistently distinguished healthy from injured lungs based on parameter estimation. Furthermore, we directly incorporate clinical and physiologic knowledge regarding important and observable features into the model that might be associated with the lung pathophysiology—the subcomponents of the model represent hypothesis-driven deviations from normal breaths. We also analytically define lung compliance in terms of model parameters and demonstrate changes in compliance values that agree with

experimentally induced lung injury. This is a proof of principle work where our objective was to develop a ventilator waveform data-based lung model and demonstrate that the model has the potential to be used both with the laboratory and clinical data and infer lung condition.

To demonstrate what is gained with this novel approach, we present a comprehensive comparison between the DILV model and the single-compartment model for a wide range of ventilator waveforms related to different lung conditions and patient-ventilator interactions. We include pressure- and volume-controlled ventilation in healthy and lung-injured mice and in humans in the absence and presence of VD. Through this comparison, we establish that the DILV model can reproduce the features present in the waveform data and report lung compliance values that agree with lung condition (**Figures 5, 6** and **Supplementary Figures 6–11**). This is primarily possible because of our unique waveform-based approach that enabled the model to have enough flexibility. At the same time, the model is limited using prior knowledge so as not to have the capability to estimate every possible variation in PV waveforms, but rather is constrained to estimate the features of the ventilator data that are the most clinically impactful. This approach lies between a machine learning approach, where the model is flexible enough to estimate every feature and must then discern which features are important through regularization to prevent overfitting, and the fully mechanistic lung modeling approach where the observed physiology must emerge from the proposed lung mechanics. It is possible that taking this middle path will help advance all approaches.

The most direct application of the DILV modeling approach is to quantify the qualitative physiological interpretation of pressure and volume data. An experienced clinician or physiologist can infer the status of a patient, the safety of ongoing ventilation, the presence of VD, and other important details from visual inspection. However, we currently do not yet have methods to identify all of these characteristics in ventilator data quantitatively. The entire waveform may be utilized and this provides a rich repository of data that is challenging and time-consuming to use for diagnosis and treatment. In contrast, summarizing the waveform data in scalar values for resistance and compliance may cast aside important details such as identifying dyssynchrony. Our approach may offer a methodology for condensing the pressure-volume data to track changes in injury severity over time, and estimate injury phenotypes (**Supplementary Figures 10, 11**). A similar phenotype study on a large dataset could be used to categorize and understand lung injury, serve as outcome measures for interventions, and describe the impacts of dyssynchrony (Sottile et al., 2018a) and VILI (Chiumello et al., 2016; Aoyama et al., 2018).

Lung injury diagnosis and decision-making are based in part on the interpretation of the pressure, volume, and flow waveforms. However, different pathophysiologic mechanisms can lead to the same observed waveform features. For example, increased driving pressure could be a result of derecruitment (alveolar collapse) or alveolar flooding (Gattinoni et al., 1987; Smith et al., 2020). In other words, the human-based inference

using limited waveform data can be ill-posed. The DILV modeling and parameter estimation approach could allow to estimate a large number of breaths efficiently with unique solutions (**Supplementary Figures 10, 11**). We could therefore use the DILV model to estimate over many similar but varied breaths, and might be able to better triangulate the most probable pathophysiologic drivers because the primary driver of damage will likely be present, and significant, despite inter-breath variations. At the same time, more extraneous details will not be consistently expressed in every breath.

Note that in the DILV model, an explicit coupling between pressure and volume signals is absent. We have intentionally taken this approach to preserve flexibility so that we can accurately recapitulate a wide variety of clinically and experimentally observed features in the pressure and volume signals, including the effects of VD (**Figures 5E,G, 6D–F**). Such flexibility in the model outcome is not always possible with rigid coupling between pressure and volume data, as we have shown by comparing the DILV model response with the single-compartment model. This is not to say that pressure and volume are totally independent in the DILV model because we utilize the same respiratory rate for both. In addition, we show that the ratio of a volume and pressure model parameter ( $A_v$  and  $A_{p1}$ ) describes lung compliance. In future studies, we will link additional specific components of the pressure and volume waveforms through physiologically relevant parameters such as the nonlinearity of lung elastance or inspiratory and expiratory flow resistance. Alternatively, a compartment-based model could be used to incorporate the physiologic coupling between pressure and volume data by utilizing the outputs from the DILV model presented here as inputs for compartment models. If the DILV model is used to preprocess the data before analysis using a compartment model, it is possible to formulate the problem entirely of ordinary differential equations, opening up a range of more efficient inference machinery (Bertsimas and Tsitsiklis, 1997; Nocedal, 2006; Albers et al., 2019b).

Finally, our work here has several notable limitations. *First*, this is a model development work, where we built a new lung model and showed that the model can accurately recapitulate waveforms and estimate accepted physiological parameters such as compliance as a baseline evaluation. This is sufficient for proof-in-principle that the model can capture physiologic differences. However, establishing that the model can accurately differentiate more specifically defined phenotypes will require validation on much larger laboratory and clinical populations. Moreover, to tie the model outputs to injury phenotypes, the pathogenesis of VILI, etc., we will have to establish the concordance between the model estimates of human and mouse-model data in similar settings and validate the phenotypes, etc., within the mouse lung. This work will be done in the following steps: hypothesize damage-related feature(s) within human ventilator, estimate model for humans and extract contextual clinical information (e.g., lung injury source), create mouse model data with a context similar to the human data, estimate the model for mice, validate concordance of model estimates between humans and mice, validate the damage severity and cause within the mice.

*Second*, the human data in this study were collected using a specific ventilator (Hamilton G5) operated in a pressure-controlled volume targeted mode. For the wider applicability of the model, additional data verification is required across different ventilators and ventilation modes. *Third*, in this work we did not explicitly relate our model parameters with the physiological or morphometric data. We rather pose hypotheses about the presence and physiological meaning of waveform features that deviate from normal instead of observing the deviant features emerging from lung physiology. For this interpretation, we relied on the expertise of a laboratory ventilation expert (BS) and a critical care physician (PS). However, it is likely that differing opinions will exist among experts. Collecting and synthesizing such information will require a different qualitative study. Moreover, there may be differing opinions regarding what should and should not be included in the model. This does not negate our novel methodology or the DILV model. In fact, the model was constructed with these issues in mind to be flexible, allowing for the testing of differing hypotheses mind. These issues suggest future work is necessary to understand better and verify clinically important features. Alternatively, we may instead seek to link model features to patient outcomes, thus establishing the important characteristics of the model by linking those parameters to outcomes. *Fourth*, in this manuscript, we have incorporated the human waveform data that has flow limited VD to demonstrated that the DILV has enough flexibility to recapitulate waveforms that have patient-VD. In order to identify and phenotype different types of VD, further model update and evaluation will be required, and this work in progress.

In summary, we developed a data-driven lung and ventilator model that can reproduce the commonly observed features in pressure and volume waveforms during mechanical ventilation. The performance of the model was verified with experimental and clinical data in healthy and injured lungs to demonstrate model efficacy in robustly estimating parameters. These parameters are hypothetically linked to both physiologic and ventilator-based mechanisms. Furthermore, the model outputs yield a pulmonary system compliance that is in good agreement with single compartment model estimates and, as expected, compliance decreases with acute lung injury. This methodology represents a departure from many lung modeling efforts, and suggests future directions of work that can provide another pathway for better understanding lung function during mechanical ventilation and can potentially form a bridge between experimental physiology and clinical practice.

## REFERENCES

- Albers, D., Levine, M., Sirlanci, M., and Stuart, A. (2019a). A simple modeling framework for prediction in the human glucose-insulin system. *arXiv* [preprint]. arXiv:1910.14193,
- Albers, D. J., Blancquart, P.-A., Levine, M. E., Seylabi, E. E., and Stuart, A. (2019b). Ensemble Kalman methods with constraints. *Inverse Problems* 35:095007. doi: 10.1088/1361-6420/ab1c09
- Albers, D. J., and Hripcak, G. (2010). A statistical dynamics approach to the study of human health data: resolving population scale diurnal variation in laboratory data. *Phys. Lett. A.* 374, 1159–1164. doi: 10.1016/j.physleta.2009.12.067

## DATA AVAILABILITY STATEMENT

The original contributions presented in the study are included in the article/**Supplementary Material**, further inquiries can be directed to the corresponding authors.

## ETHICS STATEMENT

The studies involving human participants were reviewed and approved by Colorado Multiple Institutional Review Board. The Ethics Committee waived the requirement of written informed consent for participation. The animal study was reviewed and approved by University of Colorado, Anschutz Medical Campus Institutional Animal Care Committee (IACUC)-approved protocol (#00230).

## AUTHOR CONTRIBUTIONS

DKA, BS, and DJA conception and design of the research, analyzed the data, and evaluated the model. DJA and DKA developed the mathematical model. DKA, BS, and PS designed and conducted the experiments. DKA prepared the figures and wrote the original draft of the manuscript. DKA, BS, PS, and DJA interpreted the results, edited and revised the manuscript, and approved the final version of the manuscript.

## FUNDING

This work was supported by National Institutes of Health R01 LM012734 “Mechanistic machine learning,” R01 LM006910 “Discovering and applying knowledge in clinical databases,” R01 HL151630 “Predicting and Preventing Ventilator-Induced Lung Injury” along with R00 HL128944 and K24 HL069223.

## SUPPLEMENTARY MATERIAL

The Supplementary Material for this article can be found online at: <https://www.frontiersin.org/articles/10.3389/fphys.2021.724046/full#supplementary-material>

- Albers, D. J., Levine, M. E., Mamykina, L., and Hripcak, G. (2019c). The Parameter Houlihan: a solution to high-throughput identifiability indeterminacy for brutally ill-posed problems. *Mathematical biosciences* 316:108242. doi: 10.1016/j.mbs.2019.108242
- Amato, M. B., Meade, M. O., Slutsky, A. S., Brochard, L., Costa, E. L., Schoenfeld, D. A., et al. (2015). Driving pressure and survival in the acute respiratory distress syndrome. *N. Engl. J. Med.* 372, 747–755.
- Aoyama, H., Pettenuzzo, T., Aoyama, K., Pinto, R., Englesakis, M., and Fan, E. (2018). Association of driving pressure with mortality among ventilated patients with acute respiratory distress syndrome: a systematic review and meta-analysis. *Crit. Care Med.* 46, 300–306. doi: 10.1097/CCM.0000000000002838

- Asch, M., Bocquet, M., and Nodet, M. (2016). *Data Assimilation: Methods, Algorithms, and Applications*. Philadelphia, PA: SIAM.
- Bates, J. H. (2009). *Lung Mechanics: An Inverse Modeling Approach*. Cambridge: Cambridge University Press.
- Bein, T., Weber-Carstens, S., Goldmann, A., Müller, T., Staudinger, T., Brederlau, J., et al. (2013). Lower tidal volume strategy ( $\approx 3$  ml/kg) combined with extracorporeal CO<sub>2</sub> removal versus 'conventional' protective ventilation (6 ml/kg) in severe ARDS. *Intens. Care Med.* 39, 847–856.
- Bertsimas, D., and Tsitsiklis, J. N. (1997). *Linear Optimization*. Belmont, MA: Athena Scientific.
- Blanch, L., Villagra, A., Sales, B., Montanya, J., Lucangelo, U., Luján, M., et al. (2015). Asynchronies during mechanical ventilation are associated with mortality. *Intens. Care Med.* 41, 633–641. doi: 10.1007/s00134-015-3692-6
- Cavalcanti, A. B., Suzumura, É.A., Laranjeira, L. N., de Moraes Paisani, D., Damiani, L. P., Guimarães, H. P., et al. (2017). Effect of lung recruitment and titrated positive end-expiratory pressure (PEEP) vs low PEEP on mortality in patients with acute respiratory distress syndrome: a randomized clinical trial. *JAMA* 318, 1335–1345.
- Chiew, Y. S., Chase, J. G., Shaw, G. M., Sundaresan, A., and Desai, T. (2011). Model-based PEEP optimisation in mechanical ventilation. *Biomed. Eng. Online* 10:111.
- Chiumello, D., Carlesso, E., Brioni, M., and Cressoni, M. (2016). Airway driving pressure and lung stress in ARDS patients. *Crit. Care* 20:276. doi: 10.1186/s13054-016-1446-7
- Chiumello, D., Carlesso, E., Cadringher, P., Caironi, P., Valenza, F., Polli, F., et al. (2008). Lung stress and strain during mechanical ventilation for acute respiratory distress syndrome. *Am. J. Respiratory Crit. Care Med.* 178, 346–355.
- Corona, T. M., and Aumann, M. (2011). Ventilator waveform interpretation in mechanically ventilated small animals. *J. Veter. Emerg. Crit. Care* 21, 496–514. doi: 10.1111/j.1476-4431.2011.00673.x
- Ellwein Fix, L., Khoury, J., Moores, R. R. Jr., Linkous, L., Brandes, M., and Rozicki, H. J. (2018). Theoretical open-loop model of respiratory mechanics in the extremely preterm infant. *PLoS One* 13:e0198425. doi: 10.1371/journal.pone.0198425
- Force, A. D. T., Ranieri, V., Rubenfeld, G., Thompson, B., Ferguson, N., and Caldwell, E. (2012). Acute respiratory distress syndrome. *JAMA* 307, 2526–2533.
- Gattinoni, L., Pesenti, A., Avalli, L., Rossi, F., and Bombino, M. (1987). Pressure-volume curve of total respiratory system in acute respiratory failure: computed tomographic scan study. *Am. Rev. Respirat. Dis.* 136, 730–736. doi: 10.1164/ajrccm/136.3.730
- Gelman, A., Carlin, J. B., Stern, H. S., Dunson, D. B., Vehtari, A., and Rubin, D. B. (2013). *Bayesian Data Analysis*. Boca Raton: CRC press.
- Gilstrap, D., and MacIntyre, N. (2013). Patient-ventilator interactions: implications for clinical management. *Am. J. Respirat. Crit. Care Med.* 188, 1058–1068. doi: 10.1164/rccm.201212-2214ci
- Grasso, S., Stripoli, T., De Michele, M., Bruno, F., Moschetta, M., Angelelli, G., et al. (2007). ARDSnet ventilatory protocol and alveolar hyperinflation: role of positive end-expiratory pressure. *Am. J. Respirat. Crit. Care Med.* 176, 761–767. doi: 10.1164/rccm.200702-193oc
- Grasso, S., Terragni, P., Mascia, L., Fanelli, V., Quintel, M., Herrmann, P., et al. (2004). Airway pressure-time curve profile (stress index) detects tidal recruitment/hyperinflation in experimental acute lung injury. *Crit. Care Med.* 32, 1018–1027. doi: 10.1097/01.ccm.0000120059.94009.ad
- Guerin, C. (2011). The preventive role of higher PEEP in treating severely hypoxicemic ARDS. *Minerva Anestesiologica* 77, 835–845.
- Hamlington, K. L., Smith, B. J., Allen, G. B., and Bates, J. H. (2016). Predicting ventilator-induced lung injury using a lung injury cost function. *J. Appl. Physiol.* 121, 106–114.
- Hripcak, G., and Albers, D. J. (2013a). Correlating electronic health record concepts with healthcare process events. *J. Am. Med. Inform. Assoc.* 20, 311–318. doi: 10.1136/amiajnl-2013-001922
- Hripcak, G., and Albers, D. J. (2013b). Next-generation phenotyping of electronic health records. *J. Am. Med. Inform. Assoc.* 20, 117–121. doi: 10.1136/amiajnl-2012-001145
- Jawde, S. B., Smith, B. J., Sonnenberg, A., Bates, J. H. T., and Suki, B. (2018). Design and nonlinear modeling of a sensitive sensor for the measurement of flow in mice. *Physiol. Meas.* 39:075002. doi: 10.1088/1361-6579/aa cb1b
- Jolliffe, I. T., and Stephenson, D. B. (2012). *Forecast Verification: A Practitioner's Guide in Atmospheric Science*. Hoboken, NJ: John Wiley & Sons.
- Khemani, R. G., Parvathaneni, K., Yehya, N., Bhalla, A. K., Thomas, N. J., and Newth, C. J. (2018). Positive end-expiratory pressure lower than the ARDS network protocol is associated with higher pediatric acute respiratory distress syndrome mortality. *Am. J. Respirat. Crit. Care Med.* 198, 77–89. doi: 10.1164/rccm.201707-1404oc
- Law, K., Stuart, A., and Zygalakis, K. (2015). *Data Assimilation*. Cham: Springer.
- Mellema, M. S. (2013). Ventilator waveforms. *Top. Companion Animal Med.* 28, 112–123.
- Mellenthin, M. M., Seong, S. A., Roy, G. S., Bartolák-Suki, E., Hamlington, K. L., Bates, J. H., et al. (2019). Using injury cost functions from a predictive single-compartment model to assess the severity of mechanical ventilator-induced lung injuries. *J. Appl. Physiol.* 127, 58–70. doi: 10.1152/japplphysiol.00770.2018
- Molkov, Y. I., Rubin, J. E., Rybak, I. A., and Smith, J. C. (2017). Computational models of the neural control of breathing. *Wiley Int. Rev. Syst. Biol. Med.* 9:e1371.
- Molkov, Y. I., Shevtsova, N. A., Park, C., Ben-Tal, A., Smith, J. C., Rubin, J. E., et al. (2014). A closed-loop model of the respiratory system: focus on hypercapnia and active expiration. *PLoS One* 9:e109894. doi: 10.1371/journal.pone.0109894
- Mori, K. (2016). From macro-scale to micro-scale computational anatomy: a perspective on the next 20 years. *Med. Image Anal.* 33, 159–164. doi: 10.1016/j.media.2016.06.034
- Nelder, J. A., and Mead, R. (1965). A simplex method for function minimization. *Comput. J.* 7, 308–313. doi: 10.1093/comjnl/7.4.308
- Network, A. R. D. S. (2000). Ventilation with lower tidal volumes as compared with traditional tidal volumes for acute lung injury and the acute respiratory distress syndrome. *N. Engl. J. Med.* 342, 1301–1308. doi: 10.1056/nejm200005043421801
- Nguyen, B., Bernstein, D. B., and Bates, J. H. (2014). Controlling mechanical ventilation in acute respiratory distress syndrome with fuzzy logic. *J. Crit. Care* 29, 551–556. doi: 10.1016/j.jcrc.2014.03.009
- Nocedal, J. W. S. (2006). *Numerical Optimization*. New York: Springer.
- Phua, J., Badia, J. R., Adhikari, N. K., Friedrich, J. O., Fowler, R. A., Singh, J. M., et al. (2009). Has mortality from acute respiratory distress syndrome decreased over time? A systematic review. *Am. J. Respirat. Crit. Care Med.* 179, 220–227. doi: 10.1164/rccm.200805-722oc
- Rees, S. E., Allerød, C., Murley, D., Zhao, Y., Smith, B. W., Kjærgaard, S., et al. (2006). Using physiological models and decision theory for selecting appropriate ventilator settings. *J. Clin. Monit. Comput.* 20:421. doi: 10.1007/s10877-006-9049-5
- Reynolds, A., Ermentrout, G. B., and Clermont, G. (2010). A mathematical model of pulmonary gas exchange under inflammatory stress. *J. Theor. Biol.* 264, 161–173. doi: 10.1016/j.jtbi.2010.01.011
- Rossetti, S. C., Knaplund, C., Albers, D., Dykes, P. C., Kang, M. J., Korach, T. Z., et al. (2021). Healthcare process modeling to phenotype clinician behaviors for exploiting the signal gain of clinical expertise (HPM-ExpertSignals): development and evaluation of a conceptual framework. *J. Am. Med. Inform. Assoc.* 28, 1242–1251. doi: 10.1093/jamia/ocab006
- Roth, C. J., Ismail, M., Yoshihara, L., and Wall, W. A. (2017). A comprehensive computational human lung model incorporating inter-acinar dependencies: application to spontaneous breathing and mechanical ventilation. *Int. J. Numer. Methods Biomed. Eng.* 33:e02787. doi: 10.1002/cnm.2787
- Schoukens, J., Vaes, M., and Pintelon, R. (2016). Linear system identification in a nonlinear setting: Nonparametric analysis of the nonlinear distortions and their impact on the best linear approximation. *IEEE Control. Syst. Magazine* 36, 38–69. doi: 10.1109/mcs.2016.2535918
- Serov, A. S., Salafia, C., Grebenkov, D. S., and Filoche, M. (2016). The role of morphology in mathematical models of placental gas exchange. *J. Appl. Physiol.* 120, 17–28. doi: 10.1152/japplphysiol.00543.2015
- Smith, B. J., Lundblad, L. K., Kollisch-Singule, M., Satalin, J., Nieman, G., Habashi, N., et al. (2015). Predicting the response of the injured lung to the mechanical breath profile. *J. Appl. Physiol.* 118, 932–940. doi: 10.1152/japplphysiol.00902.2014
- Smith, B. J., Roy, G. S., Cleveland, A., Mattson, C., Okamura, K., Charlebois, C. M., et al. (2020). Three alveolar phenotypes govern lung function in murine ventilator-induced lung injury. *Front. Physiol.* 11:660.
- Smith, R. C. (2013). *Uncertainty Quantification: Theory, Implementation, and Applications*. London: SIAM.

- Sottile, P. D., Albers, D., Higgins, C., McKeehan, J., and Moss, M. M. (2018a). The association between ventilator dyssynchrony, delivered tidal volume, and sedation using a novel automated ventilator dyssynchrony detection algorithm. *Crit. Care Med.* 46:e151. doi: 10.1097/ccm.0000000000002849
- Sottile, P. D., Albers, D., and Moss, M. M. (2018b). Neuromuscular blockade is associated with the attenuation of biomarkers of epithelial and endothelial injury in patients with moderate-to-severe acute respiratory distress syndrome. *Crit. Care* 22:63. doi: 10.1186/s13054-018-1974-4
- Tobin, M. J. (2001). Advances in mechanical ventilation. *N. Eng. J. Med.* 344, 1986–1996.
- Ware, L. B., and Matthay, M. A. (2000). The acute respiratory distress syndrome. *N. Eng. J. Med.* 342, 1334–1349.
- Westwick, D. T., and Kearney, R. E. (2003). *Identification of Nonlinear Physiological Systems*. Hoboken, NJ: John Wiley & Sons.
- Wheeler, A. P., and Bernard, G. R. (2007). Acute lung injury and the acute respiratory distress syndrome: a clinical review. *Lancet* 369, 1553–1564. doi: 10.1016/S0140-6736(07)60604-7
- Yoshida, T., Fujino, Y., Amato, M. B., and Kavanagh, B. P. (2017). Fifty years of research in ARDS. spontaneous breathing during mechanical ventilation. risks, mechanisms, and management. *Am. J. Respirat. Crit. Care Med.* 195, 985–992. doi: 10.1164/rccm.201604-0748cp

**Conflict of Interest:** The authors declare that the research was conducted in the absence of any commercial or financial relationships that could be construed as a potential conflict of interest.

**Publisher's Note:** All claims expressed in this article are solely those of the authors and do not necessarily represent those of their affiliated organizations, or those of the publisher, the editors and the reviewers. Any product that may be evaluated in this article, or claim that may be made by its manufacturer, is not guaranteed or endorsed by the publisher.

Copyright © 2021 Agrawal, Smith, Sottile and Albers. This is an open-access article distributed under the terms of the Creative Commons Attribution License (CC BY). The use, distribution or reproduction in other forums is permitted, provided the original author(s) and the copyright owner(s) are credited and that the original publication in this journal is cited, in accordance with accepted academic practice. No use, distribution or reproduction is permitted which does not comply with these terms.